University Of Cape Town

Masters Thesis

Measurement of Exclusive Di-Muon Production in the ATLAS Experiment

Author:
Ferdinand Schenck

Supervisor:
Dr Andrew Hamilton

A thesis submitted in fulfilment of the requirements for the degree of Masters of Science in Physics

in the

Experimental Particle Physics Group
Department of Physics

November 2015

Declaration of Authorship

I, Ferdinand Schenck, hereby declare that the work on which this dissertation/thesis is based is my original work (except where acknowledgements indicate otherwise) and that neither the whole work nor any part of it has been, is being, or is to be submitted for another degree in this or any other university. I empower the university to reproduce for the purpose of research either the whole or any portion of the contents in any manner whatsoever.

Signed:

My brothers are protons
My sisters are neutrons
Stir it twice
Instant family.

"Supertheory of Supereverything"
Gogol Bordello

UNIVERSITY OF CAPE TOWN

Abstract

Faculty of Science
Department of Physics

Masters of Science in Physics

Measurement of Exclusive Di-Muon Production in the ATLAS Experiment

by Ferdinand SCHENCK

In this thesis a method for identifying exclusively produced di-muon pairs in proton-proton collisions at the ATLAS experiment is described. The data used were collected by the ATLAS experiment at the LHC at $\sqrt{s} = 7$ TeV with an integrated luminosity of 4.6 fb^{-1}. The cross section of the process $p + \gamma\gamma + p \rightarrow p + \mu^+\mu^- + p$ was measured to be 0.98 ± 0.06 (stat.) $\pm$ 0.05 (syst.) pb compared to a theoretical prediction of 1.08 ± 0.01 (theory) pb, with a discrepancy consistent with measurement from the CMS experiment.

Acknowledgements

Firstly I would like to thank my supervisor Andrew Hamilton for all the help and support, and for helping me grow as a scientist.

I would also like to thank the National Research Foundation of South Africa for the funding provided.

Laastelik wil ek my ouers, broer en suster bedank, sonder wie se hulp en liefde dit onmoontlik sou wees om so ver te kom as wat ek sover het.

Contents

List of Figures

List of Tables

Abbreviations

LHC	**L**arge **H**adron **C**ollider
CERN	**C**onseil **E**uropéen pour la **R**echerche **N**ucléaire
ATLAS	**A** **T**oroidal **L**HC **A**pparatu**S**
CMS	**C**ompact **M**uon **S**olenoid
CDF	**C**ollider **D**etector at **F**ermilab
HERA	**H**adron-**E**lectron **R**ing **A**ccelerator
QED	**Q**uantum **E**lectro**D**ynamics
SM	**S**tandard **M**odel (of particle physics)
EPA	**E**quivalent **P**hoton **A**pproximation
RF	**R**adio-**F**requency
PSB	**P**roton **S**ynchrotron **B**ooster
TRT	**T**ransition **R**adiation **T**racker
LAr	**L**iquid **Ar**gon
DY	**D**rell-**Y**an
DDiss	**D**ouble **Diss**ociative
SDiss	**S**ingle **Diss**ociative

Chapter 1

Introduction

The Large Hadron Collider[2] at CERN provides physicists with the opportunity to study a wide variety of physical processes, some well-studied by other experiments, but also many which have previously been inaccessible due to the high energies required to observe them. The unprecedented energy and luminosity that the LHC is capable of allows for much more sensitive probing of the building blocks of our universe than has ever been available before. The LHC provides the colliding beams, but the results of these collisions are detected by the experiments placed along the LHC at the points where the collisions happen. The data obtained from these collisions can be used to test out current understanding of the laws of physics, as expressed in the Standard Model of particle physics. The Standard Model codifies the current understanding of the sub-atomic world in one theory and has been very successful so far in describing a wide variety of phenomena.

This thesis focuses on exclusive production of di-muon pairs in the LHC as detected by the ATLAS[3] detector. In this context an exclusive process is defined as an interaction in which the protons survive the interaction intact. The physical model governing exclusive interactions, Quantum Electrodynamics, is a well-understood model and allows precise testing of actual results against predictions. The case of exclusive interactions allows for a precise measurement of the Standard Model as the final state is very simple and relatively unaffected by more complex processes such as QCD interactions. An in depth description of exclusive processes can be found in Chapter 2.

In this thesis data from the 2011 run at the LHC at $\sqrt{s} = 7$ TeV centre of mass energy is used and results are compared to previous measurements by the CMS and CDF experiments.

In Chapter 2 the theory behind exclusive interactions is described, and in Chapter 3 the LHC and the ATLAS detector are described. Chapter 4 reports on the results and analysis of data, and Chapter 5 states the conclusion.

Chapter 2

Theory

2.1 Standard Model

The Standard Model (SM) of particle physics is currently the most comprehensive and well tested theory concerning the behaviour of fundamental particles. The current formulation of the Standard Model was finalised in the 1970s and combines the previously separate theories governing the electromagnetic interaction plus the strong and the weak nuclear interactions. The existence of the final undetected elementary particle predicted by the Standard Model, the Higgs boson, was confirmed by the ATLAS[4] and CMS[5] experiments in 2012.

The Standard Model predicts the behaviour of particles and their interactions, and as such predictions can be made on what the outcome of these interactions - in this case the collision of protons - will be. These predictions can then be tested against the results from experiments such as the experiments on the LHC. The Standard Model has proven to be a robust and accurate theory, with test so far confirming the predictions made by the theory. Despite its many successes there are still some questions left by the Standard Model, for example, the Standard Model does not explain the apparent matter/antimatter asymmetry observed in the universe.

The Standard Model also does not describe the functioning of gravity, although there are attempts to integrate it through a hypothetical particle called the graviton.

The Standard Model describes the interactions of all 17 elementary particles (29 if anti-particles are included) and the fundamental forces that govern these interactions, as pictured in Figure 2.1

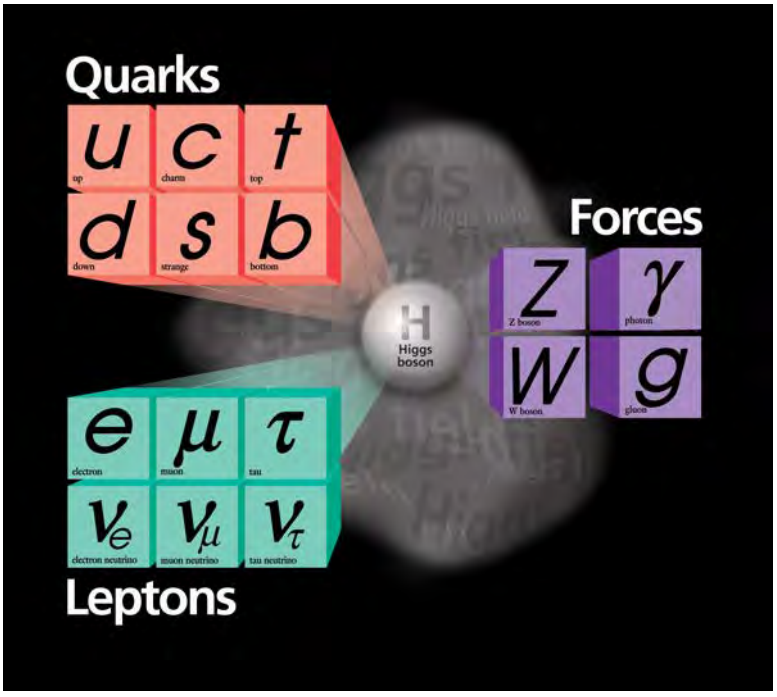

FIGURE 2.1: The Standard Model Particles [6]

The SM describes three interactions: The strong, the weak, and the electromagnetic interactions. The SM also describes the interactions of massive particles with the Higgs field through the Higgs mechanism.

The Standard Model is a local gauge invariant theory and the symmetry group over which the Lagrangian is invariant is described by the unitary product group:

$$\mathrm{SU}(3) \times \mathrm{SU}(2) \times \mathrm{U}(1)$$

Where SU(3) is the underlying symmetry group for Quantum Chromodynamics (QCD) and SU(2) × U(1) represents the unified electroweak interactions. Additionally Quantum Electrodynamics (QED) by itself is described by U(1) alone. These interactions govern all known physical interactions barring gravity.

Quantum Electrodynamics

Quantum Electrodynamics describes the interaction of charged fermions through the electromagnetic interaction as mediated by the photon, a spin-1 gauge boson. QED describes the working of the electromagnetic field through an abelian gauge theory with the underlying symmetry described by the U(1) symmetry group.

QED was the first quantum field theory and is also the simplest, with all interactions being some combination of the primitive vertex shown in Figure 2.2.

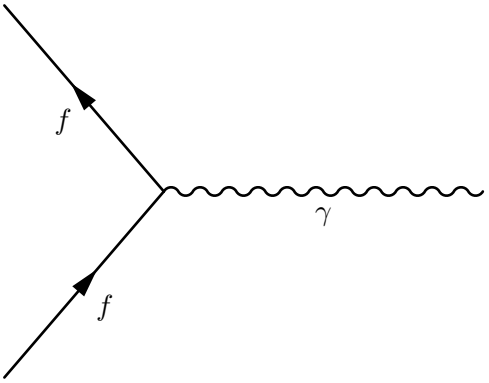

FIGURE 2.2: The basic QED vertex

An example of this would be the basic case of an electron scattering off another electron as shown in Figure 2.3, with time in this case being along the horizontal axis. In this Feynman diagram two electrons exchange a photon, which is the force carrier responsible for the repulsion the electrons will experience.

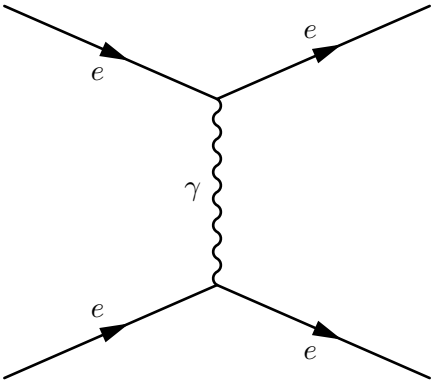

FIGURE 2.3: Electron-electron scattering

The theory is not restricted to merely simple combinations of these, but indeed to an infinite amount of combinations of the primary vertex. Every vertex, however, contributes a factor of $\approx 1/137$ (known as the fine structure constant $\alpha = e^2/\hbar c$) to the calculation, with the result that higher order processes will contribute less to the final result as order increases.

Electroweak Interactions

The theory governing electroweak interactions (EWT) has the underlying gauge group SU(2) × U(1).
Before being unified, the electromagnetic and weak interactions were thought to be two separate interactions, and were described by different theories. The electromagnetic interaction was described by Quantum Electrodynamics (QED) while the weak force was described in terms of Fermi's interaction[7]. The theories were unified by Glashow, Salam and Weinberg[8][9][10] in the 1960s and shown to be different aspects of the same interaction.

While QED describes the interaction of charged particles through the electromagnetic interaction, the weak interaction is responsible for radioactive decay and nuclear fission. The weak interaction has a limited range, implying massive charge carriers which led to the prediction and eventual discovery of the W and Z bosons. The force carriers for the electroweak interaction are thus the $W^{\pm}$ and Z bosons plus the photon. An interesting thing to thus note is that while the W and Z bosons are massive, the photon is massless. This is explained by spontaneous symmetry breaking of the gauge group. The spontaneous symmetry breaking is described by the Higgs mechanism which requires the postulation of a new field and particle, the Higgs field and the Higgs boson respectively.

The Strong Interaction

The strong interaction is described by Quantum Chromodynamics (QCD) which is a gauge theory with the SU(3) gauge group. Quantum Chromodynamics governs the interactions of quarks and gluons. Gluons couple to quarks similarly to how photons couple to electrons, but as the theory is non-abelian it allows for gluons to couple to

other gluons, thus making gluonic self-interaction possible. Analogous to electrons and photons, the quarks carry a "charge" of sorts, called colour. Unlike electric charge, which come in only one type, colour comes in three (namely red, green, and blue). Also unlike, electrodynamics the gluons carry this "charge", with gluons always having a combination of a colour plus an anti-colour. Technically the gluon will have a colour state that is a superposition of two states e.g. $\frac{r\bar{g}+\bar{r}g}{\sqrt{2}}$ where r and g represent the colours red and green.

An interesting aspect of QCD is asymptotic freedom, which results in the strong force becoming stronger with increasing distance between quarks, as opposed to becoming weaker, as is the case with the electromagnetic force and gravity. Mathematically this is expressed through the strong coupling "constant" α_s analogous to the fine structure constant of QED, although it is a running constant with the value depending on the separation distance (often expressed in terms of the magnitude of the momentum transfer, Q). In the region where α_s is small ($\alpha_s \ll 1$) the Feynman rules developed for QED can be applied perturbatively, but in the case where $\alpha_s \approx 1$ the Feynamn rules breaks down and reliance has to be made on non-analytic phenomenological models.
Another important aspect of QCD is colour confinement, which relates to the fact that free quarks are never seen in nature. Colour confinement states that quarks must be combined in colour singlet states. As quarks become separated, the force between them increases, resulting eventually in a state in which it is more energetically favourable to form a new quark/anti-quark pair for the quarks to bind with. This process, known as hadronization, results in colour neutral hadrons known as mesons and baryons consisting of two or three valence quarks respectively. Although the properties of hadrons are determined by their valence quarks, hadrons actually consist of a sea of quarks and anti-quarks. These "sea" quarks are created when the gluons responsible for carrying the strong force split into quark/anti-quark pairs. It is in general not possible to predict what fraction of a hadron's momentum is carried by which parton, and as such reliance is made on parton distribution functions (PDFs) obtained from fits to experiments such as deep inelastic scattering experiments performed by colliding protons and electrons at SLAC and HERA. These PDFs are required for cross section calculations, and as such play an important role in particle physics.

From an experimental point of view the question should be asked how we detect quarks

and gluons if they do not exist unconfined. For the most part, high momentum partons present themselves in the detectable state as a spray of hadrons, called a hadron shower. The measured properties of a hadron shower can ascertain some of the properties of the parton responsible for the shower. Hadron showers manifest themselves as jets in the detectors. More about jets in section 3.3.

2.2 Exclusive Interactions

The particular interactions of interest in this thesis, exclusive proton-proton interactions, occur when two protons interact electromagnetically but do not dissociate, i.e. break apart. The details of these interactions are predicted by Quantum Electrodynamics (QED), which is a precise theory and as a result cross sections of exclusive interactions can be predicted within an uncertainty of a few percent, mostly due to uncertainties in the protons parton distribution. The process of exclusive photoproduction of lepton pairs is rather a complicated one, but there is an approximate method that can be used to greatly simplify calculation.

The Equivalent Photon Approximation

The Equivalent Photon Approximation (EPA) is used to explain these interactions. The idea was first put forward by Fermi and developed into its current form by Budnev et al[11]. In the EPA it is recognized that the EM field of a fast charged particle becomes mostly transversely polarized with respect to the direction of motion, and at high velocities the tangential component of the EM field can be neglected. Thus the Coulomb field of a fast moving charged particle can be approximately treated as a packet of free electromagnetic waves.

In the case of lepton production a photon in the photon-flux of each proton interacts with a photon in the other and a lepton pair, in this case two muons, is formed. The cross section of the interaction can thus be treated, according to the EPA, as the well known cross section of the process $\gamma\gamma \rightarrow l^+l^-$ modified by some factor known as the equivalent photon number or spectrum[12][13]. Mathematically:

$$d\sigma_{pp\to p\ell\ell p} = \sigma_{\gamma\gamma\to\ell\ell} \otimes dN_{\gamma_1} \otimes dN_{\gamma_2} \tag{2.1}$$

where dN_{γ_1} and dN_{γ_2} represent the equivalent photon spectra for each proton, $\sigma_{\gamma\gamma\to\ell\ell}$ is the photo-production cross sections for leptons (implicitly assuming real photons), and $d\sigma_{pp\to p\ell\ell p}$ is the differential cross section of the entire exclusive proton-proton interaction

$$dN_\gamma = \frac{\alpha_{EM}}{\pi}\frac{dQ^2}{Q^2}\frac{dx}{x}\left[(1-x)(1-\frac{Q^2_{min}}{Q^2})F_E(Q^2) + \frac{x^2}{2}F_M(Q^2)\right] \tag{2.2}$$

Where:

- α_{EM} is the fine structure constant
- Q^2 is the photon virtuality (a measure of how off shell its mass is)
- $x = E_\gamma/E_p$ where E_γ and E_p are the photon and proton energies respectively
- $Q^2_{min} = \frac{m_p^2 x^2}{1-x}$ is the minimum photon virtuality with m_p the proton mass
- F_E is the electric form factor of the proton
- F_M is the magnetic form factor of the proton

In the elastic case F_E and F_M are represented in terms of the dipole approximation of the proton form factors as:

$$\begin{aligned} F_E(Q^2) &= \frac{4m_p^2 G_E^2 + Q^2 G_M^2}{4m_p^2 + Q^2} \\ F_M(Q^2) &= G_M^2 \end{aligned} \tag{2.3}$$

where G_E and G_M are the approximate dipole form factors:

$$\begin{aligned} G_E(Q^2) &= (1 + \frac{Q^2}{Q_0^2})^{-2} \\ G_M(Q^2) &= \mu_p(1 + \frac{Q^2}{Q_0^2})^{-2} \end{aligned} \tag{2.4}$$

With $\mu_p = 2.79$ is the magnetic moment of the proton in units of nuclear magnetons [14], and $Q_0^2 = 0.71$ GeV^2 the square of the dipole form factor[12].

Integrating the dN_γ terms from Q^2_{min} to Q^2_{max} gives the photon spectrum:

$$P(x) = \frac{dN}{dx}(x) = \int_{Q^2_{min}}^{Q^2_{max}} \frac{d^2N}{dQ^2 dx} dQ^2 \tag{2.5}$$

Where $Q^2_{max} = 2$ GeV is used here as in [13]. The photon spectra start behaving as $1/Q^4$ for values of $Q^2 \sim 1$ GeV resulting them becoming negligible very quickly. In fact there is very little difference in result for $Q^2_{max} = 2$ GeV and $Q^2_{max} = 100$ GeV, as is pointed out in[15].

As can be seen in Figure 2.4 the photon spectra $P(x)$ are strongly peaked at low x, meaning the photon flux of the proton will largely consist of low energy photons. Here it can be seen that a larger value of Q^2_{max} makes little difference.

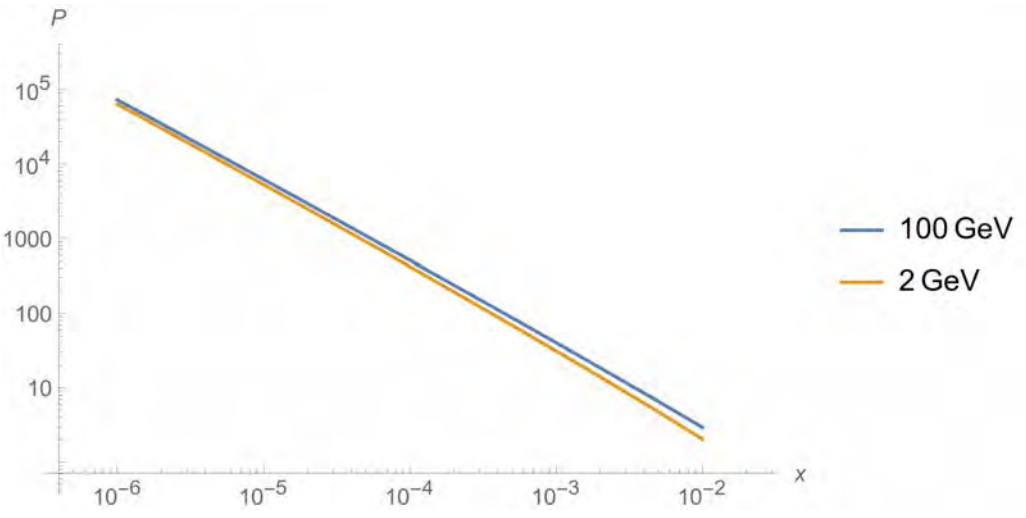

FIGURE 2.4: Number of photons as a function of fractional photon energy $x = E_\gamma/E_p$

In the inelastic case F_E and F_M are expressed in terms of the proton structure function $F_2(x_b, Q^2)$:

$$F_E(Q^2) = \int \frac{F_2(x_b, Q^2)}{x_b} dx_b$$
$$F_M(Q^2) = \int \frac{F_2(x_b, Q^2)}{x_b^3} dx_b \tag{2.6}$$

with the Bjorken scale factor $x_b \simeq \frac{Q^2}{M^2}$

In reality the photons are off mass shell and not purely transversely polarized, but in the EPA the photons in the photon flux are approximated to be massless and any non-transverse polarisation is ignored[12]. This is the essence of the approximation.

Exclusive Production

The main process that this thesis is focused on is the case of purely exclusive production of muons. In this case, two protons interact purely electromagnetically and produce two muons, as shown in Figure 2.5. As can be seen in this Feynman diagram, we expect to see two muons and two photons in the final state. However as relatively little momentum is transferred by the photons (∼10 GeV) compared to the total momentum of the proton (∼3.5 TeV), the proton is only deflected by a small angle, and thus will be "lost down the beam-pipe" i.e not interact with the detector. This makes identification challenging as two of the final state particles are for all practical purposes invisible, and the only information about the interaction comes from the two leptons.

The use of forward proton taggers (often referred to as "Roman Pots") such as the ALFA (Absolute Luminosity for ATLAS) detectors placed 240 m down the beam from the interaction point in the ATLAS detector would help greatly as the protons could be detected by these, in which case all four final state particles could be found, making reconstruction of the process much more accurate. Although the forward proton taggers would help a great deal to differentiate cases where protons did not dissociate from cases where they did, there would still be cases that "fake" our signal process, such as a case where two single dissociative interactions happen simultaneously, resulting in two intact protons in the final state, even though they were produced by different interactions.

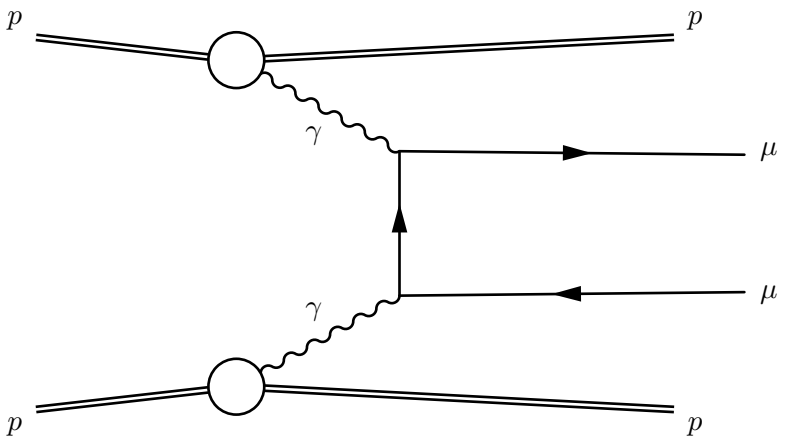

FIGURE 2.5: Feynman Diagram of the Exclusive Process

Due to the fact that we expect the central state to be produced with no significant transverse momentum, the muons are expected to be colinear in a reference frame possibly boosted along the beam-axis. This criteria can be expressed as a quantity called the acoplanarity, defined as $1 - \frac{|\Delta\phi|}{\pi}$. In Figure 2.9 it can be seen that the exclusive case is more concentrated around low values of acoplanarity. Thus by selecting only the cases with low acoplanarity we can reduce our background contribution relative to our signal.

Single Dissociative Interactions

An alternative but similar case is the case of single dissociation, i.e. when one of the protons fragments. In this case a similar process occurs, but due to energy lost by the proton it might break apart, thus fragmenting into a host of partons which then hadronise. Unfortunately, these particles are usually also not deflected by a large enough angle to be seen by the detector, rendering them practically invisible. Thus this case will look very much like our primary signal process, as only two final state muons are detected.

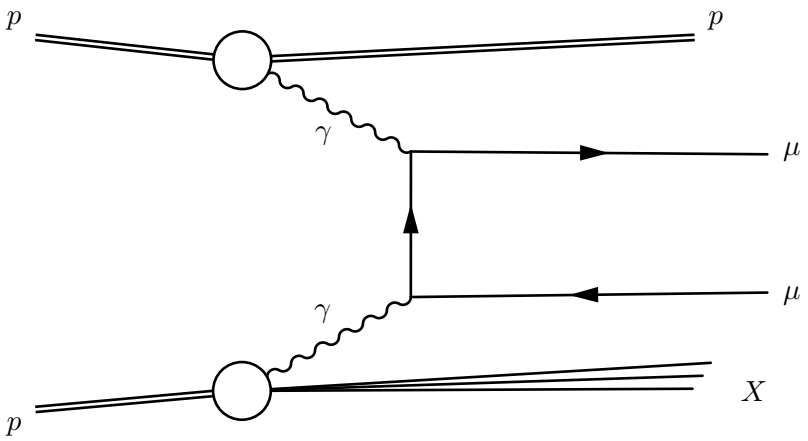

FIGURE 2.6: Feynman Diagram of the Single Dissociative Process

Again, if forward proton taggers were available it would be easier to differentiate the single dissociative case by seeing just one intact proton in the final state. Fortunately, although the single dissociative case cannot be reliably detected, the kinematic characteristics have a different distribution to that of the exclusive case, making it possible to at least reduce some of the single dissociative contribution. In particular, as there is less of a restriction on momentum transfer by the photon of the dissociating proton, the central state can be boosted in the transverse direction, resulting in a larger difference in p_T between the two muons and a larger acoplanarity than in the fully exclusive case.

Double Dissociative Interactions

Another possibility is the case where $\gamma\gamma \to \mu^+\mu^-$ but where both protons dissociate. This case is again very similar to the exclusive case and can be hard to distinguish from our signal in cases where products of the dissociation are not detected. Again the double dissociative case will form part of the background, but due to different kinematic distribution, especially in acoplanarity, a significant amount of the double dissociative contribution can be reduced.

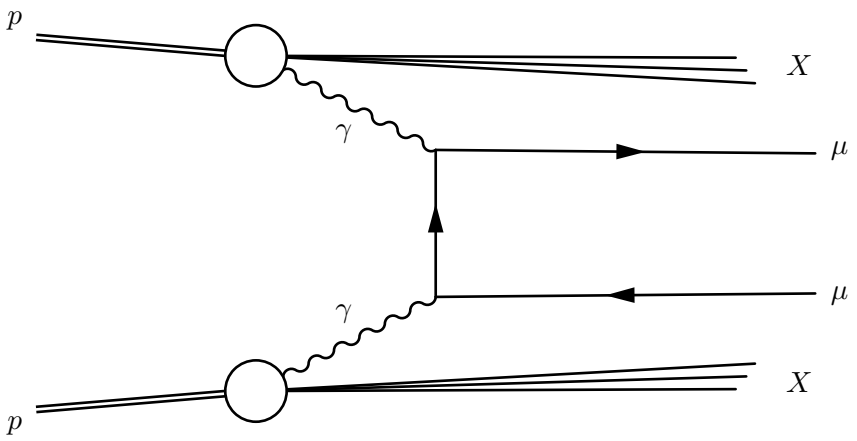

FIGURE 2.7: Feynman Diagram of the Double Dissociative Process

Drell-Yan

The background process with the highest cross-section, and thus the process that makes the highest contribution to the di-muon final state is the Drell-Yan process[16]. A Drell-Yan interaction is one where a quark in one proton annihilates with an anti-quark in the other proton, as in Figure 2.8.

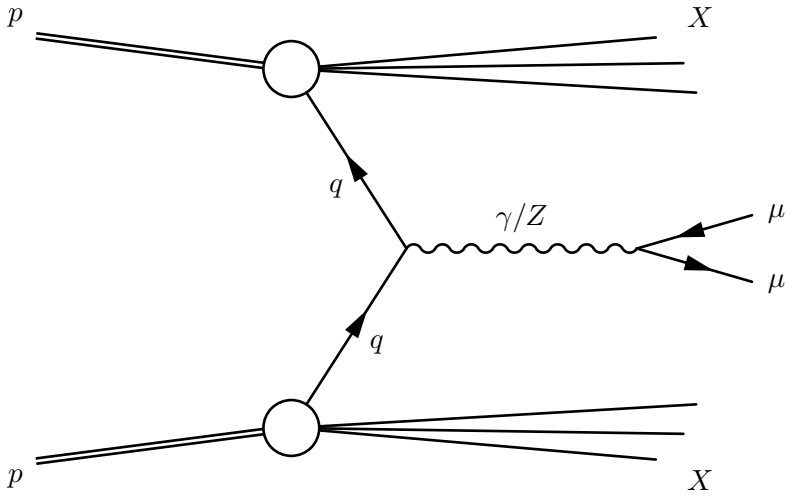

FIGURE 2.8: Feynman Diagram of the Drell-Yan Process

As can be seen in Figure 2.9, the Drell-Yan process is the most significant contributor to di-muon final states. Fortunately, as the Drell-Yan process is one where the protons collide and break apart, there are more particles in the final state which can often be seen by the detectors. Unfortunately due to the sheer amount of Drell-Yan processes that take place, there are at least some cases in which we will only see the two muons in the final state, thus making Drell-Yan part of the background. Drell-Yan processes

also lack several of the kinematic characteristics that the Exclusive process possesses, making it possible to exclude significant amounts of the Drell-Yan contribution with basic kinematic selection criteria.

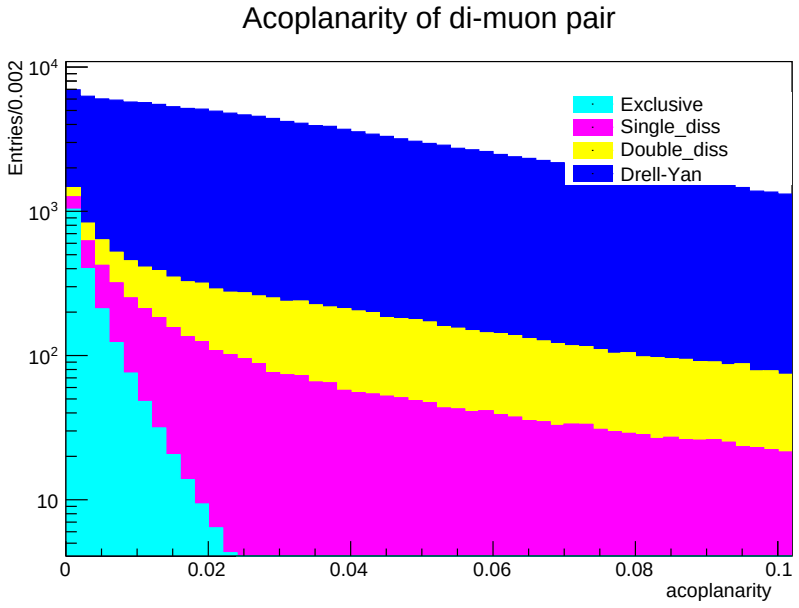

FIGURE 2.9: Full Acoplanarity of muon pairs in generator level Monte Carlo

2.3 Monte Carlo Event Generation

Monte Carlo simulations play an important part in a large fraction of modern particle physics analyses. Using theoretical models, Monte Carlo events are generated according to our understanding of the relevant laws of physics. These events thus represent what we would expect to see if nature were to work as our models describe it. Due to the probabilistic nature of particle processes, large sets of simulated events are produced in order to cover a wide spectrum of possible outcomes. These events are then fed into a simulation of a detector (the ATLAS Detector in this case, see 3 for more) from which can then be predicted what the detector would see. These simulations can then be used for various purposes, among them to test different models or detector performance. In this case they were largely used to train analysis routines before being applied to data.

The exclusive signal samples used were generated using HERWIG++ 2.5.1[17] to simulate the $\gamma\gamma \to \mu^+\mu^-$ events. The single dissociate samples were generated with LPAIR 4.0[18] for the $pp \to p{+}\mu^+\mu^-{+}p*$. For the double dissociative samples and the Drell-Yan

samples PYTHIA8[19] and LPAIR 4.0 were used to simulate the $pp \to p* + \mu^+\mu^- + p*$ and $q\bar{q} \to \gamma* \to \mu^+\mu^-$ processes[20].

2.4 Survival Factor

The models governing the behaviour of exclusive interactions employed by the Monte Carlo generators neglect the finite size effects of the proton. While this was a good approximation for lower energies, at LHC energies this approximation starts to break down.

The Monte Carlo generator used to produce the exclusive and single dissociative samples, LPAIR, does not account for finite size effects, and as such is expected to overestimate the exclusive and single dissociative cross section. To explain this estimation, a survival factor has been defined that takes into account the structure of the proton.

The survival factor gives an indication of how likely a proton is to survive an photon mediated interaction and is related to the energy of the photon in relation to the energy of the proton. In Figure 2.10 the fraction of the proton energy carried by the photons is shown as x_1 and x_2. As can be seen, the survival factor decreases with increasing photons energy. In the related study[21] it was found that the survival factor for LHC energies should be around 0.8, meaning it is expected that the Monte Carlo should overestimate the exclusive and single dissociative cross sections by about 25%.

2.5 Previous Measurements

Previous measurements of the exclusive production of lepton pairs have been made by the CMS[22] and CDF[23][24] experiments. In [23] the CDF experiment studied the exclusive production of e^+e^- pairs. Here 16 events were observed and the cross section was found to be $1.6^{+0.5}_{-0.3}$(stat.)$\pm$0.3(syst.) pb which agrees with the theoretical prediction of 1.71 ± 0.01 pb.
In [24] CDF studied the exclusive production of muon pairs, and observed a cross section of 2.7 ± 0.3(stat.)$\pm$0.4(syst.) pb compared to a prediction of 2.18 $\pm$0.01 pb.

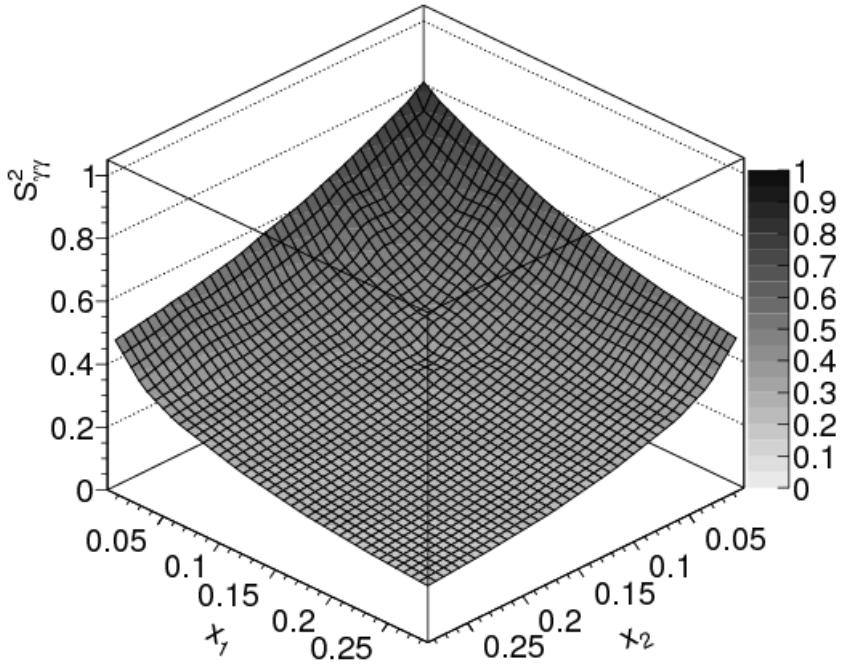

FIGURE 2.10: Survival Factor

In the CMS measurement of muon pairs the cross section was found to be $3.38^{+0.58}_{-0.55}$(stat.)$\pm$0.16(syst.)$\pm$0.14(lumi.) pb. Here the measured cross section was smaller than predicted by the theory by a factor of 0.83, attributed to the fact that the Monte Carlo generator used (LPAIR) does not take the proton structure into account. Interestingly for the CDF measurement on muons, while still within 1σ of the predicted measurement, the Monte Carlo seems to underestimate the measured cross section.

Chapter 3

The LHC and the ATLAS Detector

3.1 The LHC Accelerator Chain

The Large Hadron Collider (LHC)[2] is currently the world's largest and most energetic particle collider and is located near Geneva on the border between France and Switzerland.

The LHC was designed to collide protons at a centre of mass energy of $\sqrt{s} = 14$ TeV in a 27 km long ring of superconducting magnets used to control the proton beams. Two beams of protons travel around the ring in opposite directions at close to the speed of light and are made to collide at four intersections where detectors are placed in order to observe the products of these collisions.

The LHC was built with the purpose of testing the predictions of the Standard Model of particle physics as well as probing beyond the Standard Model theories such as Supersymmetry.

There are four main detectors on the LHC: ATLAS, CMS, LHCb and ALICE.

There is a significant amount of work that goes into accelerating bunches of protons to TeV scale energies, and it is impossible for a single accelerator to achieve this. The LHC itself receives the protons with energy already at 450 GeV and accelerates them to the final energy, which was designed to be 7 TeV, although the LHC was run at 3.5 and 4

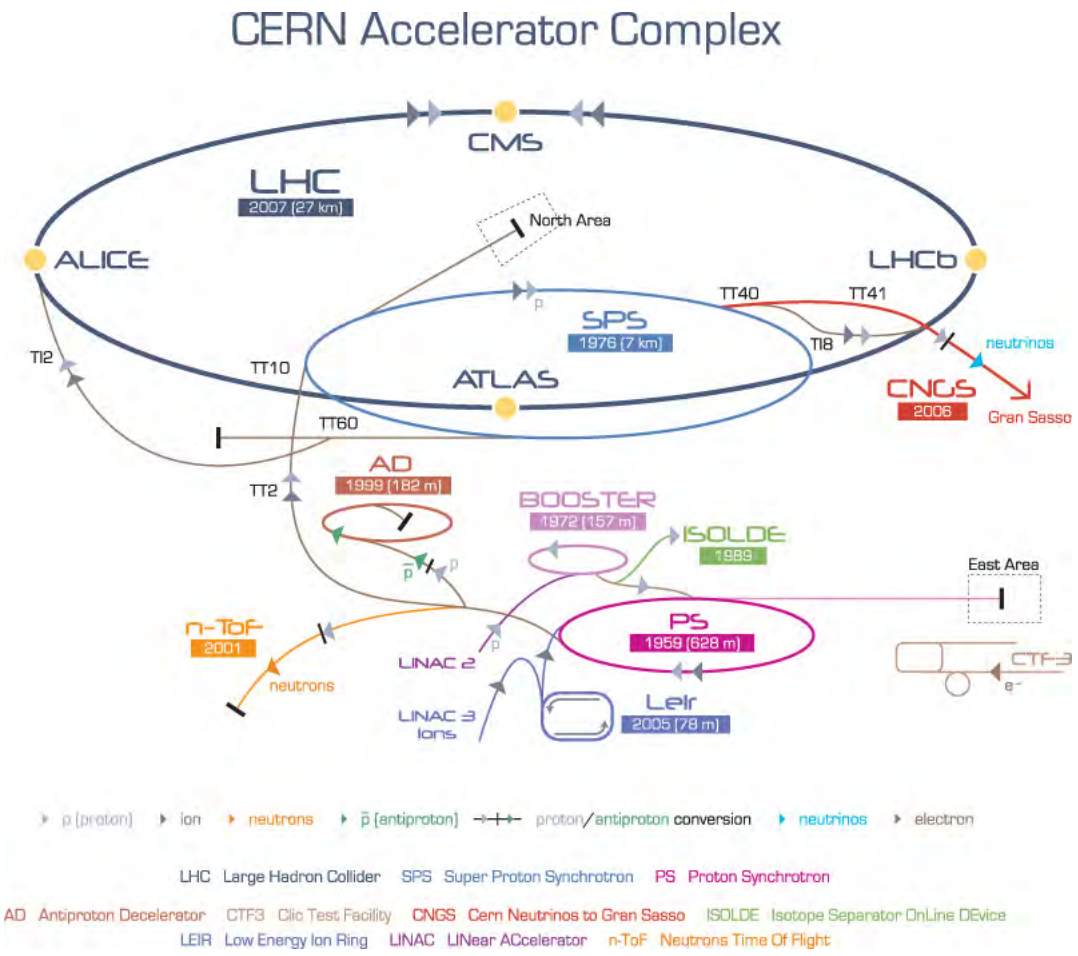

FIGURE 3.1: The LHC Accelerator Complex[25]

TeV for run I, and run II at 6.5 TeV with a possibility of reaching the design energy later in the run. There is a chain of smaller accelerators that consecutively accelerate and then pass on the bunches of protons that will eventually be collided in the LHC. This chaining of accelerators is necessary as every accelerator has a limited range of operating energies. In principle one could build a linear accelerator that could bring the protons up to 14 TeV and then inject them into the LHC purely for collision, but this would be an extraordinarily long and expensive machine. The main reason circular accelerators are favoured over linear accelerators in very high energy experiments such as the LHC and the Tevatron is that in a linear collider each part of the accelerator is used only once, meaning that for higher energies you would need a longer accelerator. In the case of circular colliders, the same piece of hardware can be used over and over at increasingly higher energies, thus making them much more cost (and space) effective solutions. This does however come with some drawbacks. Circular accelerators are of limited use when accelerating low mass particles such as electrons and positrons, as the

energy loss due to Bremsstrahlung during the bending of the beams becomes a limiting factor. Fortunately for heavier particles such as protons or heavy ions, this effect is much smaller (the charge to mass ratio is the important factor). However, due to the fact that the electromagnets that are used to bend the particles in a circle have particular operating ranges, it means that the energies that a synchrotron collider can handle are also constrained to a particular range. Usually these circular colliders have an energy range of a bit more than an order of magnitude. For example, the LHC itself accepts protons at 450 MeV and accelerates them up to a maximum of 7 TeV, thus roughly a 20 fold gain in energy.

Below is a description of the major steps in the LHC accelerator chain also pictured in Figure 3.1.

The Duoplasmatron

The first step to be taken is to acquire free protons. The process starts with hydrogen gas that is injected into a duoplasmatron, in which there is a filament which acts as a cathode and from which electrons are emitted, and which is surrounded by an intermediate electrode which acts as the anode towards which the electrons are accelerated. Inside this plasma chamber (between the cathode and the anode, as can be seen in Figure 3.2) the hydrogen gas is injected. A magnetic field is applied such that the magnetic field lines are parallel to the sides of the chamber. The electrons spiral around the chamber and can now ionize the hydrogen gas, resulting in free protons. The plasma chamber is connected to another chamber of a higher vacuum but with a strong magnetic field applied to it. When some of the plasma escapes into the extraction chamber, the negative and positive ions are separated by the electric field, with the protons being extracted and the electrons being pushed back towards the plasma chamber. These free protons are now fed into a linear accelerator known as Linac2.

Linear Accelerator

The linear accelerator consists of several radio-frequency (RF) cavities which consist of cylindrical conductors which are alternately positively and negatively charged. The charge on the cylindrical conductors is rapidly varied at radio-frequency resulting in

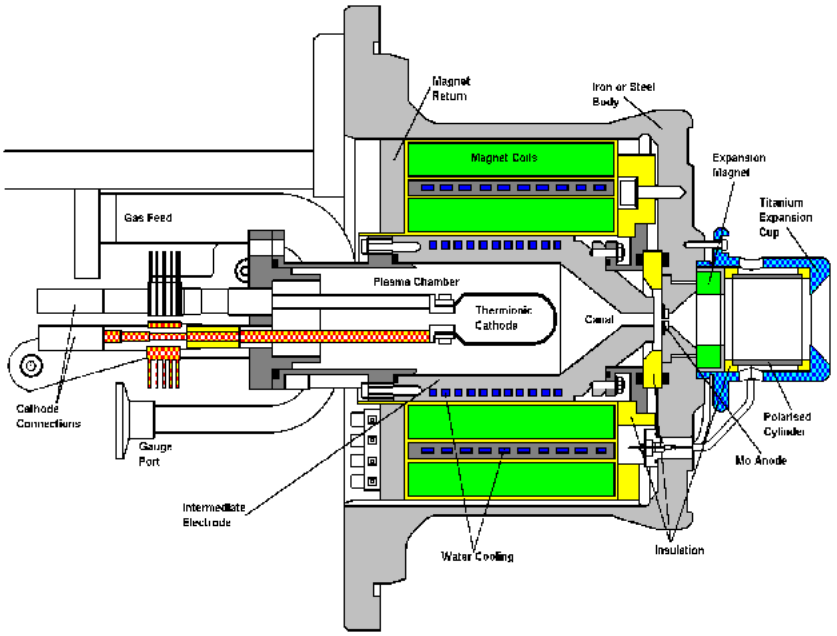

FIGURE 3.2: The Linac2 Duoplasmatron[26]

electric fields which pull/push charged particles. The protons from the duoplasmatron are injected into the linear accelerator which accelerates them up to an energy of 50 MeV and then passes them on into the booster rings of the Proton Synchrotron Booster.

Booster

The Proton Synchrotron Booster consists of four stacked synchrotron rings. Due to the fact that the linear accelerator can produce much higher luminosities than most synchrotrons can handle, a packet of protons from Linac2 is split up into four parts and put into the PSB, where the protons are accelerated from 50 MeV to 1.4 GeV. The PSB works in a similar way to the LHC (which is just a large synchrotron), by keeping the protons in control with magnets, and by accelerating the protons in stages with radio-frequency cavities. It is during this stage that the protons are forced into tight groups, called bunches.

Proton Synchrotron

From the PSB the proton bunches are sent to the Proton Synchrotron, where the particles are further accelerated, now increasing the energy of the protons from 1.4 GeV to

25 GeV.

Super Proton Synchrotron

After the Proton Synchrotron, the protons are sent into the penultimate stage, the Super Proton Synchrotron (SPS), which now increases the energy of the protons from 25 GeV to 450 GeV. In the SPS the bunches of protons are all circulating in the same direction, unlike the LHC, where there are two pipes with beams running in opposite directions. From the SPS the bunches are injected into the LHC, with half the packets being injected into each of the two beams.

The Large Hadron Collider

The Large Hadron Collider is a synchrotron proton collider with two beam pipes in which bunches of protons are accelerated in opposite directions and which intersect at four points. The LHC uses superconducting magnets with magnetic field strength of about 8 Tesla at full power to keep the beam in a circular trajectory. For run I, i.e. 2010-2012, protons circled the detector in 1374 bunches per beam, less than the design value of 2808. The bunch crossing rate was designed to be 40 MHz with 25 ns bunch spacings, but in run I a 20 MHz interaction rate with 50 ns bunch spacings was used.

3.2 The ATLAS Experiment

The ATLAS experiment is a general-purpose detector on the LHC designed to detect a wide variety of the interactions that occur in high energy hadron collisions. The detector is 25 meters in diameter, 46 meters in length, and weighs around 7000 tonnes.

The ATLAS detector consists of several sub-detectors optimised to detect certain types of particles. The detector is roughly cylindrical in shape with the different sub-detectors of the detector forming concentric sections. See Figure 3.3. The component closest to the beamline, and thus the interactions, is the inner detector which tracks charged particles originating from collisions in the beam-pipe. Surrounding this is the electromagnetic calorimeter which detects electrons, positrons and photons and captures and measures the energy that they carry. Surrounding the electromagnetic calorimeter is the hadronic

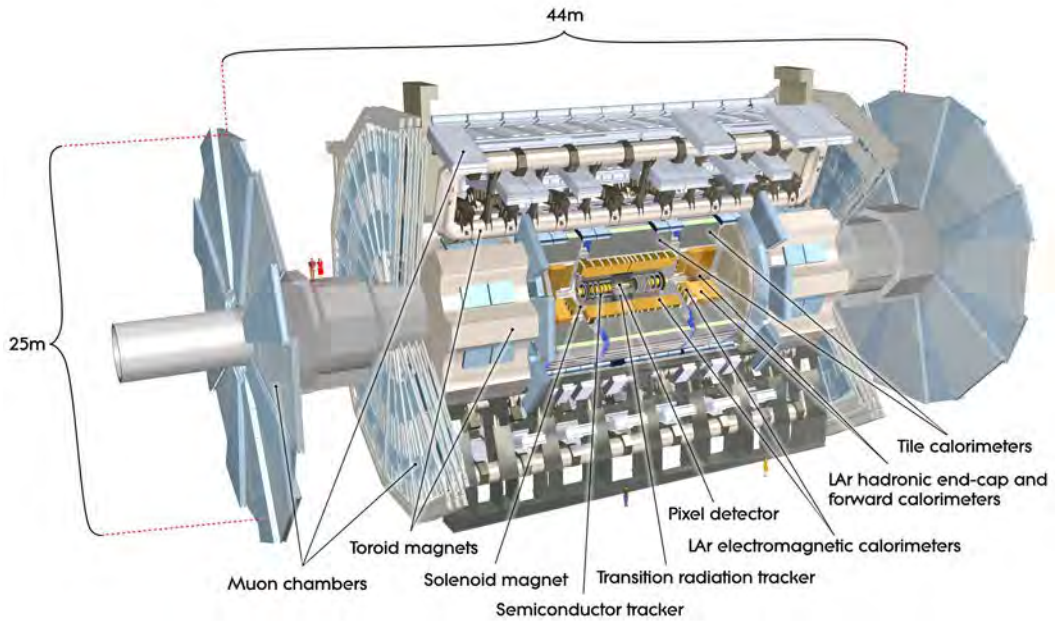

FIGURE 3.3: The ATLAS Detector[27]

calorimeter which detects hadrons (such as protons and pions). Lastly the outermost section is the muon spectrometer, which is used detect muons, which mostly escape the detector without being stopped. This section will describe the principles by which the detectors work and ties into the section 3.3 where the signatures left by particular classes of particles passing through the detectors are described.

The coordinate system of the ATLAS detector is defined with the z-coordinate along the beam-axis with the positive z in the anti-clockwise direction (when the ring is considered from above), with the $z = 0$ set to the middle of the ATLAS detector along the z-axis, where the nominal interaction point is located. The x coordinate points inwards towards the centre of the LHC ring, and the y coordinate is perpendicular to both x and z. The angle ϕ is defined as the angle in the transverse (xy) plane, with $\phi = 0$ on the x-axis. The angle θ is the angle as measured from the z-axis, but is in practice replaced by the pseudorapidity, $\eta = -\ln\tan(\theta/2)$, and is preferred as particle production is roughly constant in pseudorapidity.

Tracking Detectors

The purpose of a tracking detector is to collect information about the passage of charged particles in such a way that the information gathered can be used to reconstruct which path the particle followed as it passed through the tracking detector. This information is used to construct a "track" for the particle, which can be used to match it to identified particles in the electromagnetic and hadronic calorimeters and can be used to calculate the momentum of the particle.

To achieve this, a tracking detector must be able to record detailed spacial information about the path of a charged particle. In order to calculate the momentum of the particle, a magnetic field needs to be applied in order to force the charged particle to move in a curved path. By knowing how much a particle curved under the influence of a magnetic field one can calculate the momentum that the particle was carrying.

The tracking detector in the ATLAS experiment consists of a silicon pixel detector, Semiconductor Tracker (SCT) and a Transition Radiation Tracker (TRT) [28] that lie within a superconducting solenoid magnet with a field strength of 2 Tesla parallel to the beam axis.

The silicon pixel detector is the closest to the beam pipe and consists of layers of silicon pixels. A charged particle passing through the pixel detector might interact with a pixel, resulting in a signal. As the detector is calibrated, the position of each pixel is well known, a path for the track of the particle can be reconstructed assuming enough of the pixels were hit.

The SCT comes after the pixel detector and consists of strips of silicon, with every layer consisting of two arrays of strips oriented at a stereo angle of 20 μrad with respect to each other. This offset allow for positioning information to be reconstructed if several of the layers see a signal.

The Transition Radiation Tracker (TRT) of tightly packed drift tubes that are filled with a gas (70% Xe, 27% CO_2 3% O_2) with a golden wire in the center of the tubes. A charged particle traversing the barrier between the inside and outside of a drift tube produces photons through a process known as transition radiation. The passage of the charged particle as well as the photons produced through transition radiation ionises

the gas, thus releasing electrons that move towards the gold wire in the center of the tube, resulting in a measurable signal. The magnitude of this signal is dependent on the amount of ionisation that happens, and as different charged particles will result in different amounts of photons as they move through matter, it is possible to identify different particles this way.

As the position of these drift tubes are also well known due to calibration, the TRT provides accurate tracking information about the path of the charged particle. Thus together with the pixel detector, the path that a charged particle takes can be reconstructed. A lot of useful information can be gained from knowing the path of a charged particle. As there is a magnetic field present in the detector, a charged particle will follow a curved path when moving through the field. The trajectory of the particle will be indicative of the sign of the charge of the particle as well as the transverse momentum carried by the particle.

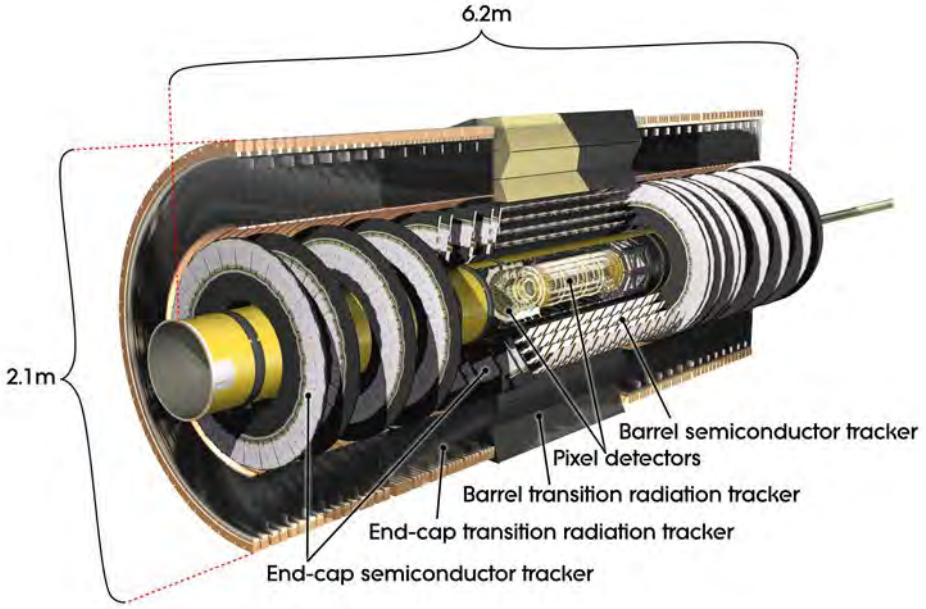

FIGURE 3.4: The ATLAS Inner Detector[29]

Calorimeters

Calorimeters are devices that fully absorb the energy carried by a particle, and are instrumented in such a way that the energy absorbed by the device can be measured. The two main classes of calorimeters are electromagnetic calorimeters and hadronic calorimeters, the details of which are discussed below. Both types of calorimeter work on the basis of interacting with the particle in such a way that a shower (electromagnetic or hadronic) is started. Each particle produced in this shower will have a lower energy than the one preceding it, resulting in the shower eventually stopping within a few interaction lengths. Thus it is important for calorimeters to be thick enough to reliably capture the full energy of a particle, but without being so thick as to interfere with particles that need to pass through it. For example, the electromagnetic calorimeter should be thick enough to fully absorb the energy carried by an electron or photon, but not so thick that it would significantly impede the passage of hadrons which need to reach the hadronic calorimeter.

Quantitatively the above condition for "thick enough" can be described in terms of radiation lengths (X_0) and nuclear interaction lengths (λ). The radiation length of a material is characteristic to the material and can be approximately expressed as[30]:

$$X_0 = \frac{716.4g \cdot cm^{-2}A}{Z(Z+1)\ln\frac{287}{\sqrt{Z}}} \tag{3.1}$$

Where Z is the atomic number of the material and A the mass number. After one radiation length a charged particle will have its energy reduced by a factor of $\frac{1}{e}$ due to radiative losses. X_0 is also $\frac{7}{9}$ of the mean free path of a high energy photon in the material, after which the photon will pair produce a electron/positron pair. The EM calorimeter is over 22 radiation lengths thick in the barrel, and over 24 radiation lengths in the end-caps[2].

The nuclear interaction length for a material can be approximately expressed as[30]:

$$\lambda \approx 35g \cdot cm^{-2}A^{\frac{1}{3}} \tag{3.2}$$

and is the distance after which all but $\frac{1}{e}$ of a beam of hadron will interact with the material. The ATLAS detector has about 9.7 λ of active calorimeter in the barrel region and 10 λ in the end-caps, with a full thickness of 11 λ at $\eta = 0$ if inactive material is included[2].

Thus again the question of "thick enough": for hadrons after ∼10 interaction lengths lengths only $(\frac{1}{e})^{10} \approx 0.004$ % of hadrons will not have interacted with the calorimeter. This is a relatively small fraction and very few hadrons will pass through the calorimeter without interacting. For the electromagnetic case 22 radiation lengths means that $(\frac{1}{e})^{22} \approx 3 \times 10^{-8}$ % of charged particles will pass through without interacting. With such a small fraction it can essentially be guaranteed that no electron or photon will pass through without interacting.

There are two main classes of calorimeter: homogeneous calorimeters and sampling calorimeters.
A homogeneous calorimeter, as the name implies, consists of only one type of material that is responsible both for capturing the particle's energy and for generating a signal. Sampling calorimeters on the other hand consist of an absorber material that initiates a particle shower, and a separate material used for creating a signal such as a scintillator. Both of the Calorimeters used in the ATLAS detector are sampling calorimeters.

Electromagnetic Calorimeter

Electromagnetic calorimeters measure the energy lost via electromagnetic interactions by particles passing through the detector. An ideal electromagnetic calorimeter would completely absorb photons and electrons/positrons while allowing hadrons to pass through. Materials used in electromagnetic calorimeters are thus chosen based on their ability to absorb different types of radiation. In an electromagnetic calorimeter photons would primarily interact via pair production of electrons and positrons, while electrons and positrons would lose energy via Bremsstrahlung.

The electromagnetic calorimeter in the ATLAS experiment is located radially outside the tracking detector. The detector is made up of an accordion grid structure of steel

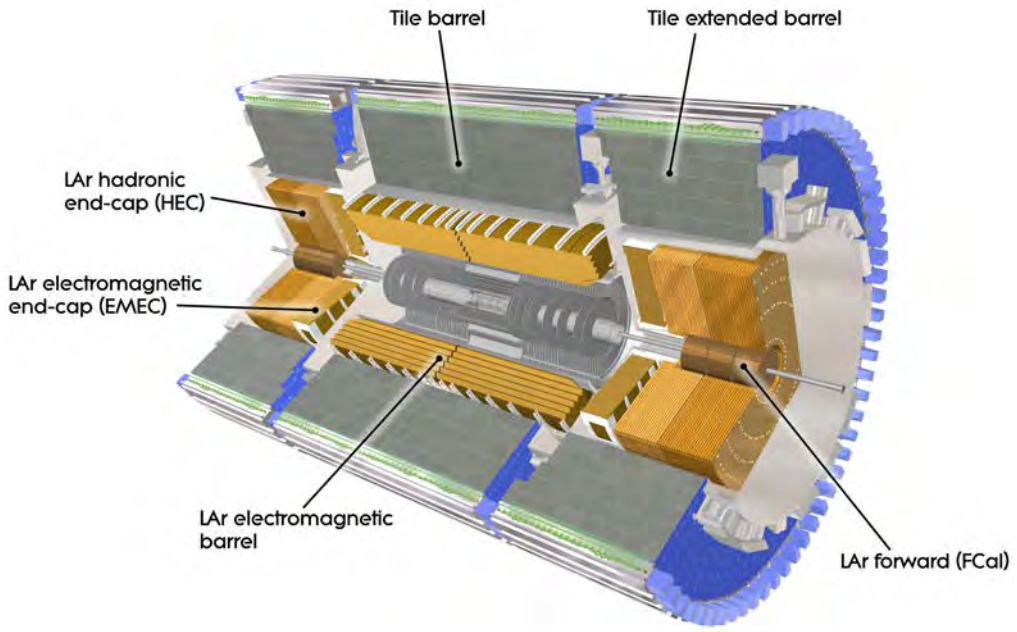

FIGURE 3.5: The ATLAS Calorimeters[31]

and lead plates immersed in Liquid Argon (LAr) with a copper grid inside to carry away the signal. A high energy electron/positron will interact with the steel and lead to produce a shower of photons and electrons/positrons which can then again interact with another layer of material, while a high energy photon will interact with the matter in the detector and pair-produce an electron-positron pair. These secondary particles will then repeat this process until the energies become to low to produce more particles. Charged particles moving through the detector will ionize the liquid Argon, resulting in electrons that will drift towards the copper grid, resulting in a signal. The amount of total energy deposited by a particle can then be inferred from the total amount of signal measured by the calorimeter, as higher energy particles will produce larger signals.

The calorimeter is designed to be thick enough that it is unlikely that a particle will pass through the calorimeter without depositing all of its energy, although this is possible, and is known as "punch-through".

Hadronic Calorimeter

Hadronic calorimeters are used to measure the energy carried by a hadron, thus the focus of the materials chosen for the detector material would be those that will have a high probability of interacting with hadrons via the strong force, in other words a

more dense material. In an ideal hadronic calorimeter a hadron would deposit all of its energy in the calorimeter, which would absorb the energy in such a way that the energy deposited can be accurately determined. Hadrons passing through a material will result in hadronic and electromagnetic showers.

The detector is made up of interleaved sheets of steel and scintillating material. The interaction of a hadron with the nuclei of the steel results in a shower of charged particles, which then move through the scintillator. Charged particles moving through the scintillator result in light being produced, which can then be measured. The amount of light created by the interaction of a hadron with the calorimeter is proportional to the amount of energy carried by the hadron, thus the energy of the hadron can be deduced by the amount of light detected by the calorimeter.

Hadronic interaction length is longer than electromagnetic interaction length, meaning a thicker calorimeter is needed to minimize punch-through.

Muon Spectrometer

The purpose of the muon spectrometer is to detect the passage of muons through the detector. Like electrons, muons lose energy through Bremsstrahlung when interacting with matter, but due to the fact that the muon has a much larger mass than the electron the effect of Bremsstrahlung is much smaller. Taking a look at Figure 3.6 it can be seen that in copper the energy loss of muons at momenta of ∼100 MeV/c to ∼1000 GeV/c is very small[32]. Due to this fact muons pass through the entire detector virtually unhindered. As muons are charged, muons will have their tracks bent by the magnetic field of ATLAS and will ionise the matter that they pass through, meaning they will leave tracks in the detector systems. As a large portion of the muons created by collisions have energies ranging from several hundred MeV to single TeV, stopping muons in calorimeters in order to measure their energy is impossible (at least for detectors smaller than several kilometres in diameter), thus the energy of the muons have to be calculated some other way. As the probability that any other charged particle can pass through all the previous layers of detector and into the muon spectrometer is very low, we can be relatively certain that any charged particle that makes it to the muon spectrometers is a muon. The muon fake rate is estimated to be of the order of 1 in 1000 for muons with

p_T above 5 GeV[3]. By carefully measuring the track of the muon the momentum can be calculated.

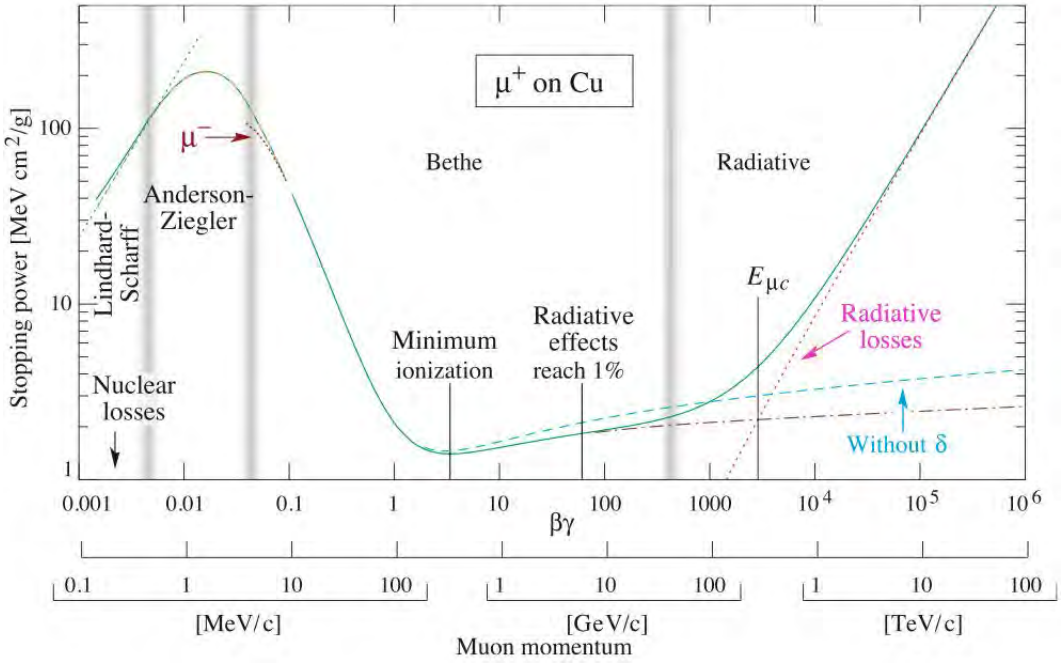

FIGURE 3.6: Muon Energy Loss [32]

The muon detector again employs drift tubes to measure the passage of the (charged) muons. As in the TRT, the muons ionise the gas in the drift tubes, resulting in a signal if the spectrometer is hit. The muon spectrometer consists of 1200 of these chambers filled with drift tubes, making up an area of 12 000 m^2. The chambers are housed within a toroidal magnet system with a field strength of between 2 and 8 Tesla, which results in the muon having a curved path from which the sign of their charge and the magnitude of their transverse momentum can be deduced.

3.3 Signatures

Although there are many particles created during collisions in the LHC comparatively few are long lived enough to actually make it to the detectors. However, the particles that are long lived enough to be detected have certain signatures by which they can be identified, and in many cases a collection of detected particles with certain kinematic characteristics can be indicative of a shorter lived particle decay.

A so-called "signature" of a particle is a collection of signals from one or more of the sub-detectors that is indicative of the passage of a certain particle. Below is a discussion of the main signatures observed by the ATLAS detector.

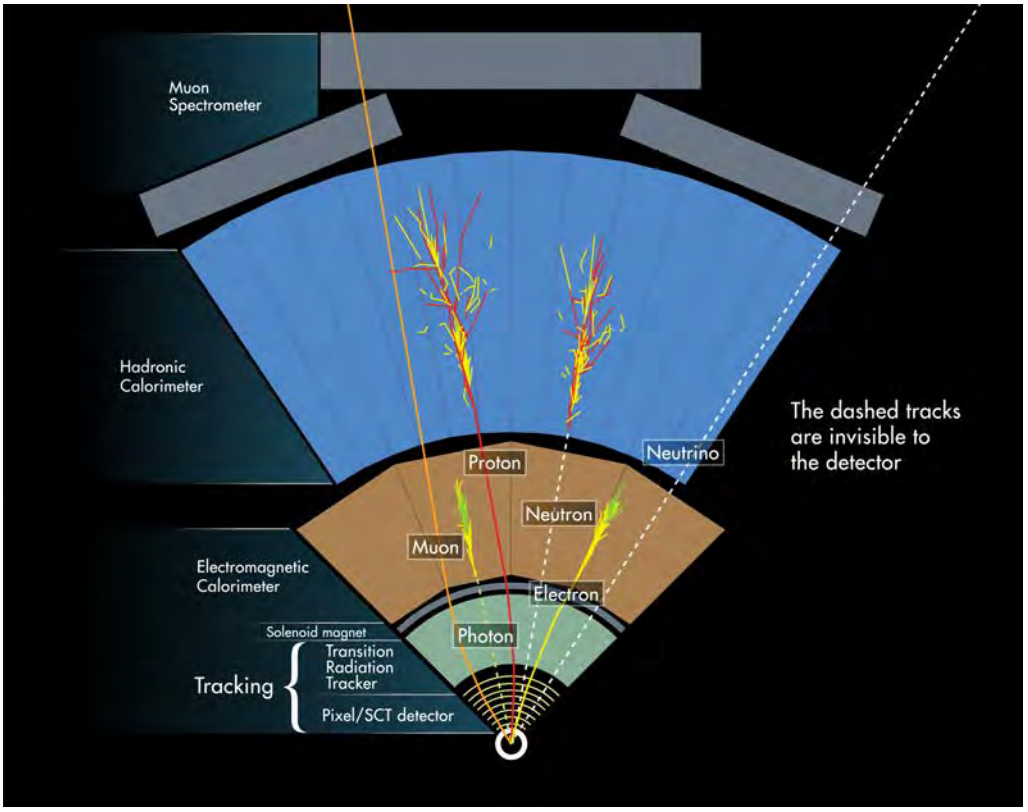

FIGURE 3.7: ATLAS Side View[33]

Electrons and Photons

An electron created in a collision (with enough p_T) will travel through the SCT, and as it is charged, will leave pixel hits when it passes through a pixel. Next it will pass through the SCT and TRT, again leaving signals. Because the positions of the components in the TRT, SCT and silicon pixel detector are well known, the signal the electron leaves in these components allows for accurate reconstruction of the path the electron takes, usually called its track. Finally, the electron hits the electromagnetic calorimeter. The characteristic signature of an electron in the electromagnetic calorimeter is a large shower of lower energy electrons which are absorbed and which leave a total signal proportional to the energy carried by the electron.

A photon(γ) leaves a similar signal in the electromagnetic calorimeter as an electron, as a γ will pair produce an electron positron pair, which will then create a cascade of lower energy electrons thus resulting in a similar signature as for an electron. The big difference in identification is the lack of a track in the silicon detector, SCT and TRT. Due to the lack of track there is more uncertainty when reconstructing the origin of a γ when compared to a charged particle.

Muons

The muon (μ) signature is the main signature being used in this investigation.

Muons are an interesting case as they easily pass through matter with minimal interaction, and escape the detector without being stopped, thus using a calorimeter to capture the energy carried by a muon would be impossible. Thus some other method must be found to reconstruct the energy carried off by a muon. Firstly, as we know a muon is the only charged particle that can traverse all layers of the detector, we can be reasonably certain that any particle seen by the muon spectrometer is indeed a muon. Secondly as a muon ionises the matter it passes through, a muon will leave a signal in all the sub-detectors it passes through. Thus, as the muons track can be accurately reconstructed, and thus the radius of its curvature in the magnetic field can be accurately measured, the momentum of the muon can be obtained.

A muon travelling through the detector first interacts with the SCT, as it is a charged particle. Next, the particle travels through the TRT, where it again leaves a signal, much in the same way an electron would, although due to the inverse mass dependence on the amount of transmission radiation emitted, a smaller signal will be observed.

The important distinction comes next, at the calorimeters. Most particles are stopped by the calorimeters, while the muon passes straight through with very little interaction. As shown in Figure 3.6, the stopping power of matter for muons is very low.

Finally, the muon interacts with the muon spectrometer at several points before leaving the detector.

As the muons leave signatures in many levels of the detector, from the silicon detector and TRT to finally the muon spectrometer, the track of the muons can usually be

accurately reconstructed from the many points of interaction. The fact that the muon is charged and thus curves when in the detector's magnetic field means that the curve of the track will tell us the sign of the charge of the muon as well as the momentum of the muon. An accurate measurement of the track will result in an accurate reconstruction of the momentum.

One interesting case to take into account is the case of cosmic ray muons. As the detector is located 100m underground the detector is shielded from most particles. However muons, which can travel through a large amount of matter, can reach the detector, especially through the access shafts, which have relatively little shielding. Therefore, as the cosmic ray muons move in a straight line they can be misidentified by the detector as coming from a collision, as they are back to back and have no other tracks, thus having some of the signatures of an exclusive signal event.
There are several ways of preventing cosmic ray muons from being identified as muons coming from collisions.

1. The position of the track in relation to the beam axis can be considered. Any cosmic ray muon that passes through the detector far from the beam axis can easily be discarded as a cosmic ray.

2. Precise timing can be used. It would be expected that if two muons were created in a collision that they would pass through the detectors at nearly the same time, while for a cosmic ray muon the timing of when the particle moves through the detectors should necessarily be different.

3. Lastly, a cosmic ray will look to the detector like two opposite sign muons travelling in perfectly opposite directions. Thus, by excluding muons with opening angles very close to 180° we can exclude cosmic ray muons. This is the method used in this analysis.

Jets

Quarks and gluons are produced in many of the collisions that happen in the LHC, but due to confinement these particles never reach the detectors. Although these particles never make it to the detectors, they hadronise into an array of lower momentum particles,

usually resulting in a shower of particles hitting the detectors. As four-momentum is conserved, the mass of the original particles can be reconstructed from the products.

A jet is seen when a particle hadronises and results in a shower of several particles being detected in the trackers and calorimeters. A characteristic of a jet is a relatively tight grouping of particles. Due to the mechanics of hadronisation the final state particles will be a shower of particles with lower energy than the original particle. Thus this shower needs to be identified and grouped in order to regain the original particle's characteristics.

Tau

The Tau (τ) particle, the heaviest lepton, has a very short lifetime. The τ decays hadronically two thirds of the time, and leptonically the other third. In the case of the leptonic decay only a lepton (an electron or a muon) is detected in the final state, while one or two neutrinos are created but are never detected and could result in a missing momentum being "detected" by the detector. In the case of a hadronic decay, several (between 2 and 4) pions and a tau neutrino are in the final state. The presence of neutrinos make precise measurement of tau decays much harder than those of its lighter siblings.

MET

Missing transverse energy (E_T) occurs when the vector sum of the transverse energy in the interaction does not sum up to zero. The main cause of missing E_T occurs when neutrinos are created in interactions and carry away a significant amount of energy. By looking at the momenta of the detected particles coming from a collision the missing energy in the transverse plane can be calculated. The main way of doing this is to look for cases where the detected particles do not conserve p_T, and then to reconstruct how much momentum was "lost" and in which direction. This can then be used to estimate the momentum of this invisible particle. The case of one neutrino is not so problematic, but cases with more than one could result in high uncertainties in energy. Missing E_T can also come about due to detector effects such as cracks in the detector, jet calibration, or could be as a result of exotic particles such as dark matter.

b-jet

A lot of interesting physical processes involve b-quarks (bottom or beauty), e.g. Higgs decays or top decays. The b-quark is the second heaviest of the quarks, but is also relatively long-lived for a particle of its mass. Because of this lifetime, the b-quark can travel a significant distance before it hadronises, leading to a secondary vertex around 500 micrometers from the original vertex. This displaced vertex is a signature of a b-jet.

Bottom quarks, being heavy, also have the property of decaying to a large number of particles, on average 5 charged particles. Thus a large number of tracks is also characteristic of a b-quark decay. Often a lepton is also produced; another signature. Thus a combination of these is good evidence for a b-quark.

3.4 Simulation

The event simulations described in Chapter 2.3 so far only describe the physical processes and do not take into account the response of the detector. The response of the detector, due to geometry and efficiencies is simulated by GEANT4[34]. GEANT4 is a detector simulation software package that is used to model how the detector would react to the passage of particles. The events generated from the theory are then passed to a GEANT4 based simulation of the ATLAS detector, which simulates how the detector should respond to particles passing through the various components of the detector. The output from this simulation mirrors the output that would be received from the real detector, allowing the same analysis code to analyse the Monte Carlo or data in the same manner, ensuring that the logic applied to both is the same.

Chapter 4

Analysis

In this chapter the measurement of the exclusive $\gamma\gamma \to \mu^+\mu^-$ production cross section is reported. The measurement was done using 4.6 fb^{-1} of LHC proton-proton data collected in 2011 using the ATLAS detector. This analysis has been done in parallel with a larger ATLAS analysis[35].

When two beams of particles collide many types of interactions might occur. Some interactions are relatively common while others are more rare. These probabilities are usually expressed in terms of a characteristic cross section of an interaction, measured in units of area. While units of area sound like a strange way to quantify interaction probability there are valid reasons for doing so. Historically particles were thought to be hard spheres and the larger the size of a particle (and thus its cross section) the more likely particles in a beam of particles would interact with it. Today cross section is still used as it is independent of many beam parameters (e.g. intensity), and this independence makes it easier to compare results from different experiments. Cross sections are usually expressed in terms of barns(b), where 1 b = 10^{-28} m^2.

A cross section at a collider experiment can be expressed as:

$$\sigma = \frac{N_s}{A\varepsilon \int \mathcal{L} dt} \tag{4.1}$$

where N_s is the amount of signal events observed for a given amount of data, A is the acceptance, ε is the efficiency of identifying these signal events, and $\int \mathcal{L}dt$ is the integrated luminosity.

The integrated luminosity is, as the name suggests, the luminosity of a collider integrated over time. The luminosity of a collider depends on the beam parameters, such as the beam width and particle flow rate, and is the proportionality factor between the cross section and the number of events per second, $\frac{dN}{dt} = \mathcal{L}\sigma_p$. The integrated luminosity thus gives us the amount of particles that might have collided in a given time and is thus used as a measure of how many interactions might have happened, or how much data was collected.

The efficiency ε is a measure of how effective a detector is at detecting a particle. Essentially the efficiency tells us the fraction of particles that were detected out of all the particles that hit the detector. The acceptance A of the detector tells us the ratio of particles that hit the detector over the amount of particles emitted. The acceptance is due to the geometrical outlay of the detector and is thus dependant on the trajectory of the particle.

In modern particle physics experiments it is rare that any real conclusions can be drawn from measuring the products of only one particle collision. This is due to the fact that for a large fraction of interactions, the measurable final state is not unique and several types of interactions will result in identical final states. Here the concepts of signal and background can be introduced. The signal is the type of interaction being considered by the study, in the case of this analysis the signal would be the exclusive photo-production of muon pairs. The backgrounds would be all the processes that might result in similar final states, such as single dissociative processes described in Chapter 2. In order to compensate for the fact that signal and background events might be indistinguishable, many modern particle physics experiments rely on colliding huge numbers of particles, and by making statistical deductions from the observed data. Another property of particle interactions is that many interactions have several possible outcomes, some of which might be very rare; thus a large number of collisions is required in order to observe these rare interactions.

An example of how an analysis might proceed is the case of finding evidence for the existence of a new particle, e.g. a Higgs boson. In such a case one or several decay

channels are considered, for example the case in which a Higgs boson decays into two photons. Unfortunately the Higgs boson is not the only possible interaction that might result in a two-photon final state, meaning that we can never be sure if any specific two-photon final state was produced by the decay of a Higgs boson. But by predicting how many two-photon final states we expect to see in a given amount of data if no Higgs boson was present, either gleaned from theoretical predictions or from some data-driven technique (as was the case with the two-photon channel), a significant excess of two-photon final states can confirm the existence of a new particle. This can be done by measuring some characteristic property of the interaction, a distinguishing variable, such as the invariant mass of the system. This will be a variable for which it is possible to distinguish the signal from the background. The Higgs boson has a set mass and will appear as a resonance in the invariant mass spectrum, thus comparing the expected invariant mass against the invariant mass found evidence for a new particle will show up as an excess in final states with a specific invariant mass. By measuring the "size" of this excess (i.e. the frequency with which new particle appears) the cross section of this interaction can be ascertained. This cross section can then be compared to theoretical predictions and either exclude certain theories or lend credence to others.

Most particle physics analyses follow this general pattern, with the details of which characteristic property and which final states being considered varying greatly.

4.1 Outline of Analysis Strategy

The extraction of the cross section requires us to look at all data in which muons were detected. As such we consider the ATLAS muon stream for 2011, which contains all collisions in which at least one muon with sufficient momentum was detected. As one of the goals of this study was to extend a CMS analysis on 2010 data[22], but with higher statistics, the 2011 data set was considered. As part of the CMS analysis, all beam crossings that resulted in more than one collision were vetoed and only those with a single collision were kept, thus resulting in a no pile-up environment. As instantaneous luminosity increases the average number of collisions per bunch crossing also increases, with the result that very few bunch crossing will result in a single collision, making the requirement used by CMS inefficient at higher luminosities. One of the goals of this study was to test whether an analysis like this one would be possible at higher pile-up

conditions it was decided to use only 2011 data.
To put the challenge into numbers, it should be considered that the 2011 data contains about 300 billion collisions and we are expecting that only about 7500 muon pairs to be exclusively produced. Thus we are looking for a very small signal in a very large data pile. On this data selection criteria based on the kinematics of the physical process being studied as well as detector efficiencies are applied. This data is then compared to predictions from the Monte Carlo, on which the same selection criteria has been applied. The information we need from the Monte Carlo is the selection efficiency, i.e. which portion of our signal events are actually identified as such, and to know which portion of our final events are expected to be from the signal process and which are from background processes.

As discussed in Chapter 2 several Monte Carlo generators were used to generate our different signal and background samples. For the exclusive signal HERWIG++ 2.5.1 was used, but as HERWIG++ 2.5.1 cannot simulate the dissociative process LPAIR 4.0 was used to simulate the single dissociative sample. For the double dissociative sample two generators were available, the legacy LPAIR 4.0 generator and the more modern PYTHIA8. Note: PYTHIA8 could not be used for single dissociative samples as PYTHIA8 cannot at this time handle non-fragmented protons. For the Drell-Yan background PYTHIA8 was used as well.

It is important to discuss how the double dissociative background was handled. There are two generators available to handle the production of the double dissociative samples, PYTHIA8 and LPAIR 4.0. Both of these generators were considered for the analysis. As in the official ATLAS publication[35] PYTHIA8 was used as the main generator, but LPAIR 4.0 was used as a cross check to see if the results obtained were similar. A discrepancy between the two generators could have indicated a problem with different implementations of the physical models, but no significant discrepancy was found. The two double dissociative generators were used differently. For the LPAIR 4.0 case, during the fitting process the single and double dissociative samples were scaled together as one contribution. The reasoning behind this is that the same model governs the behaviour of the single dissociative and double dissociative processes, and that if the model describes one of the processes inaccurately, it should also describe the other with a

similar discrepancy. For the PYTHIA8 case, the double dissociative is kept fixed whereas the single dissociative is free to vary. The reasoning behind this is that PYTHIA8 is a more modern generator and tuned for the LHC. There are large uncertainties in the double dissociative samples due to the uncertainties in the photon PDFs[36], and these are taken into account in the systematic uncertainties where it is shown that even a significant variance in the double dissociative sample has only a small effect on the final result.

4.2 Event Selection

As there is a large amount of data being analysed, criteria have to be identified to select the data which is needed and to exclude that which is not, based either on the measurable characteristics of our signal process, or on criteria due to the functioning of the detector system.

The data used were required to pass the criteria of being in a 2011 "good runs list": The good runs list contains information pertaining to when the detector was fully functional, and by using only data specified by this list it can be assured that the results obtained are not affected by malfunctioning hardware.

In order to effectively extract signal events from the total set of data we have to relate the physical processes to what is actually seen by the detector.

From the physics of exclusive production we know that a $\mu^+\mu^-$ pair will be produced. Thus our first criteria is that we only consider events in which there are at least two muons. Secondly, as we have a muon and an anti-muon, we must ensure that the particles have opposite charge. Next, as the particles must come from the same interaction it is necessary to perform a check that they are indeed reconstructed back to the same vertex by the detector.

We know that in the exclusive case the central state produced by the two photons should not be significantly boosted in the transverse plane. A result of this is that we expect our final state muons to have very similar transverse momenta. Another result of this

lack of boost is that we expect the muon pairs to be "back-to-back" in ϕ, i.e. the plane transverse to the beam-axis. We can test this by requiring that the muon pairs have low acoplanarity, where we define acoplanarity as $1 - |\frac{\Delta\phi}{\pi}|$.

Another case we have to take into consideration is contamination due to cosmic ray muons. A cosmic ray muon passing through the detector at the right position might pass all of the selection criteria mentioned thus far, as a μ^+ moving through the detector in one direction will look very much like a μ^- moving in the other direction. Also, as cosmic rays are necessarily back-to-back they look very much like our signal. Thus in order to counter this we implement a cut on the three-dimensional opening angle of the muon pair, to ensure that we do not misidentify a cosmic ray muon as a signal event.
This analysis has been restricted to an invariant mass window of 20 to 60 GeV, largely to avoid the more complex Z-region as the Z-boson can decay into a muon pair.

During the 2011 run a trigger was in place for di-muons that only selected for di-muon pairs where both muons have more than 10 GeV of momentum, thus only muons with p_T above 10 GeV can be safely considered. This criteria was also enforced on the Monte Carlo to ensure consistency.

In addition to applying selection criteria based on the underlying physical process being investigated we also need to consider the limitations of the detector. Any detector has some constraints to consider in order to obtain an accurate picture of the processes being detected. These limitations may stem from detector geometry or from accuracies of the detector system.
The first constraint we have to consider is the pseudorapidity region which is instrumented in the detector. As the detector is cylindrical with a space for the beam pipe there will necessarily be a region of the detector that cannot be instrumented. As a result there are certain trajectories to which the detector will be effectively blind. Consider Figure 4.1. Here is the reconstruction efficiency for muons as a function of pseudorapidity. The efficiency for reconstructing muons is very high within the $|\eta|$ smaller than 2.5, but declines significantly outside of this region, thus we implement a cut of $|\eta|$.

Some additional criteria to ensure the fidelity of the muon signal were applied. These criteria are:

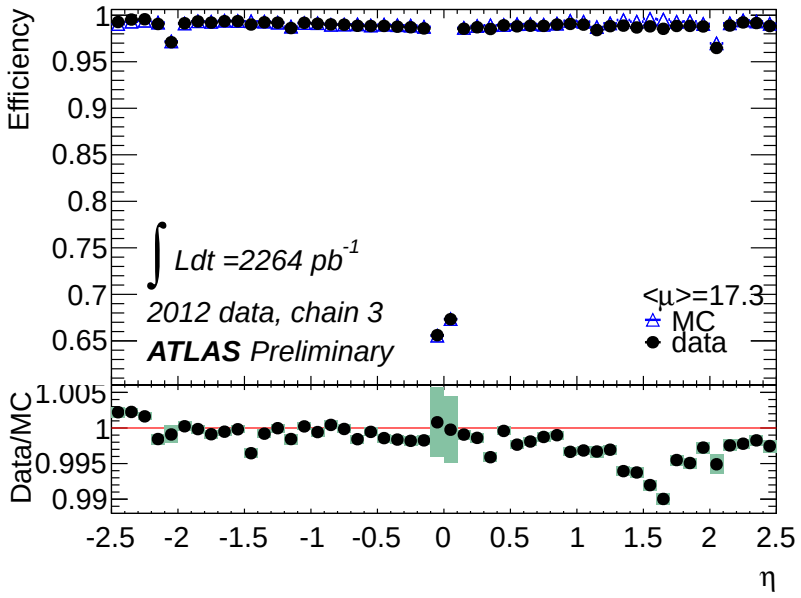

FIGURE 4.1: Reconstruction efficiency for combined+segment tagged muons versus the muon pseudorapity.(η)[37]

An isolation requirement on the muon track to ensure that the muon was not produced by a jet. The requirement it that within a cone of $\Delta R < 0.2$, $\Sigma p_T/p_T^\mu < 0.1$, where $\Delta R^2 = \Delta\phi^2 + \Delta\eta^2$, and p_T/p_T^μ is the total transverse momentum in the cone divided by the transverse momentum of the muon alone. This requirement makes sure there are no other high p_T tracks close to the muon.

A minimum number of hits in the inner detector are required namely:

- At least one hit detected in the first layer (known as the BLayer) of the SCT, if the reconstructed trajectory should produce a hit.
- At least one hit in the pixel detector, with dead pixels included if the track's trajectory traverses any.
- At least 5 hits in the SCT, including dead strips traversed.
- Less than 4 holes in the pixel detector and SCT combined, where holes are pixels or strips traversed by the reconstructed track but with no signal found.
- The number of hits plus the number of outliers in the TRT must be larger than 4
- The ratio of outliers/(outliers + hits) in the TRT must be smaller than 0.9

The last two requirements are only valid in the region $0.1 < \eta < 1.9$. Outliers in the TRT occur when there is activity in a straw near a track in the TRT but there is no track with a reconstructed trajectory should pass through the straw. Outliers also occur when there is activity in TRT straws that do not form a smooth trajectory with a track projected from the SCT and pixel detectors.

The ATLAS tracking system reconstructs tracks then identifies vertices from which the particles originated. The system for doing this has a limited accuracy, thus the tracks of vertices which are closer to each other than the detector resolution can possibly be reconstructed. Thus we apply a cut to ignore any instances where vertices or stray tracks appear too close to the vertex of interest. Table 4.4 provides a summary of the major selection criteria applied.

TABLE 4.1: Signal Selection Criteria

Parameter	Accepted Values
tracks per vertex	$\equiv 2$
Δp_T	< 1.5 GeV
Acoplanarity	< 0.01
θ_{3D} (cosmics)	$< 0.95\pi$
$M_{\mu\mu}$	20-60 GeV
$\lvert\eta\rvert$	< 2.4
p_T	> 10 GeV
vertex exclusivity	$= 3$ mm

The number of events that pass the selection criteria are listed below in Table 4.2.

TABLE 4.2: Cut Flow Table

Selection Criteria	Data	Exclusive	Single Diss.	Double Diss.	Drell-Yan	Total MC
Preselection	7559306	4411	8929	5206	1444490	1463035
Same vertex	62492	1111	2241	1330	21003	25686
Two Tracks	4497	948	1901	1122	1087	5058
Vertex exclusivity	3347	907	1820	1072	639	4438
Δp_T	2214	888	1087	409	302	2687
Acoplanarity	1168	830	400	72	38	1340

As can be seen there is initially a large discrepancy (there is almost twice as much data as MC), but the cut on tracks per vertex makes a significant difference and results in the theory and data being similar. This is attributed to several backgrounds not taken into account in this thesis, but more fully studied in the official ATLAS publication[35]. As can be seen in Figure 4.2 the selection criteria of only two tracks per di-muon vertex excludes all backgrounds except those considered in this analysis. Of these backgrounds, the QCD background is the most significant. The other significant backgrounds are due to the Drell-Yan production of τ pairs which decay leptonically, di-bosons (W^+W^-, ZZ or $W^\pm Z$) which decay leptonically as well as $t\bar{t}$ production in which the top quarks might decay into a W or Z boson which then decays into a leptons.

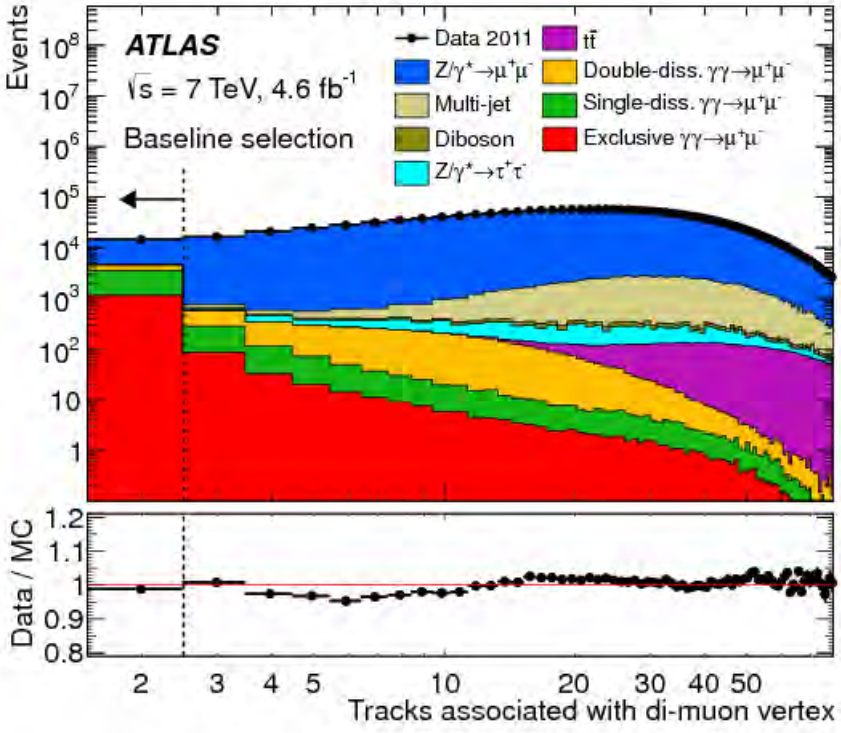

FIGURE 4.2: Number of tracks associated with di-muon vertices[35]

4.3 Signal Extraction

For muon pairs with invariant mass between 20 to 60 GeV, with muons having transverse momenta of at least 10 GeV, there are 1168 muon pairs that pass our selection criteria. From the Monte Carlo samples normalized to 4.6 fb^{-1} of data, we expect 830 of these

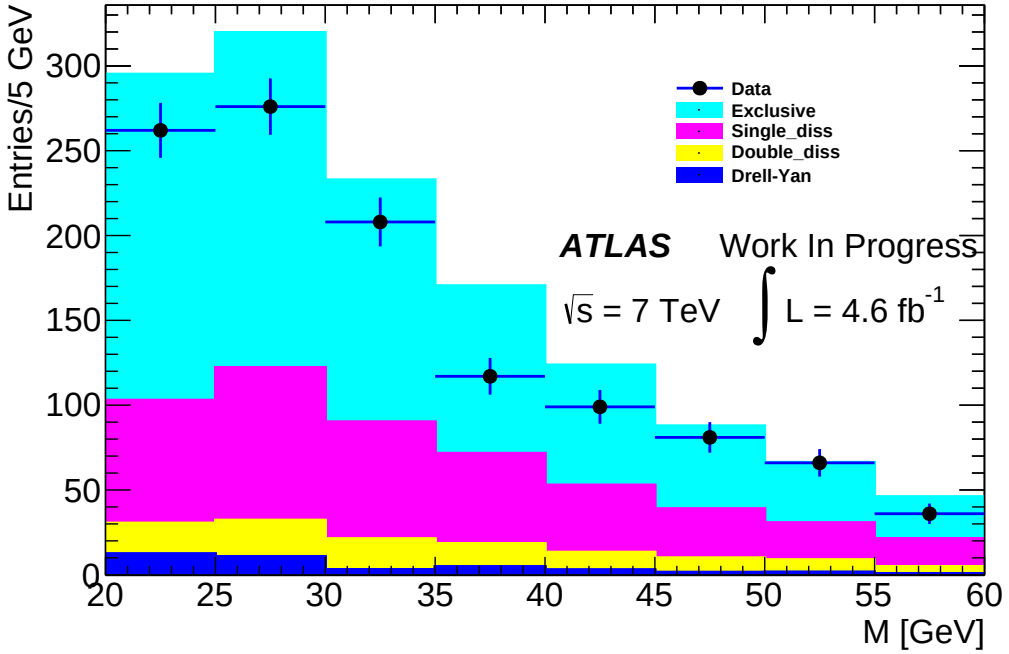

FIGURE 4.3: Invariant mass of the di-muon pair before application of scaling factors

to be from fully exclusive processes. As can be seen in the number of events and Figure 4.3 this is a overestimation by the Monte Carlo.

This discrepancy was also reported by CMS[22] and predicted in[21]. In order to quantify this discrepancy the Monte Carlo was scaled to fit the data. The fitting done was a fractional fit, in which the shapes of the Monte Carlo sample's probability distribution functions (PDFs) were extracted, and then the relevant contributions were simultaneously fit to the data. Note that PDF here is different from PDF in Chapter 2 which is also the acronym of parton distribution function. The fit was done using RooFit[38]. To ensure that the fit is sensible a parameter must be chosen in which the shapes of the different PDFs are distinguishable. As shown in Figures 2.9 and 4.4, the different samples have different shapes in the acoplanarity, and thus it was chosen as the fitting parameter. Fits were first attempted with all except the exclusive contribution kept fixed, but this does not result in a satisfactory fit. The same was done with only the single dissociative allowed to vary, but again this does not produce a good fit, indicating that in both samples the cross sections are not well modelled by the generators. In the analysis by CMS, both the single dissociative and exclusive contributions were allowed to vary while the double dissociative and Drell-Yan samples were kept fixed.

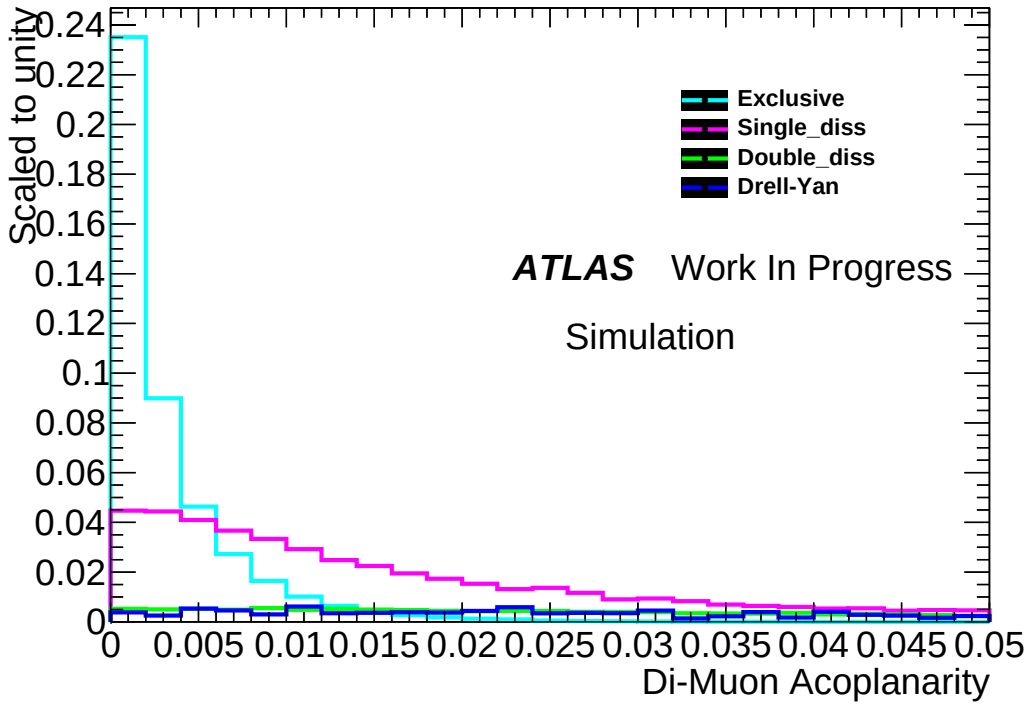

FIGURE 4.4: Shapes of Probability Distribution Functions of the signal and background contributions from simulation. PDFs of Double Dissociative and Drell-Yan are small and similarly shaped.

As described before, in this analysis two paths were taken with the two different generators. The cases will be referred to as the PYTHIA8 case and the LPAIR 4.0 case. For the LPAIR 4.0 case the single and double dissociative cases were scaled by the same amount, as well as letting the exclusive vary, while for the PYTHIA8 case the exclusive and single dissociative samples were let vary while the double dissociative and Drell-Yen were kept fixed.

For the PYTHIA8 case the ratio between what is predicted and what is found from the fit is $R^{ex}_{data/mc} = 0.91$, while the ratio for the single and double dissociative cases was found to be $R^{sdiss}_{data/mc} = 0.72$. In order to check the agreement of the Monte Carlo and the data, the important kinematic variables are compared. The acoplanarity is plotted in Figure 4.5 with the above ratios applied.

For the case with LPAIR 4.0 double dissociative the ratios were $R^{ex}_{data/mc} = 0.88$ and $R^{diss}_{data/mc} = 0.76$, and this is plotted in Figure 4.6.

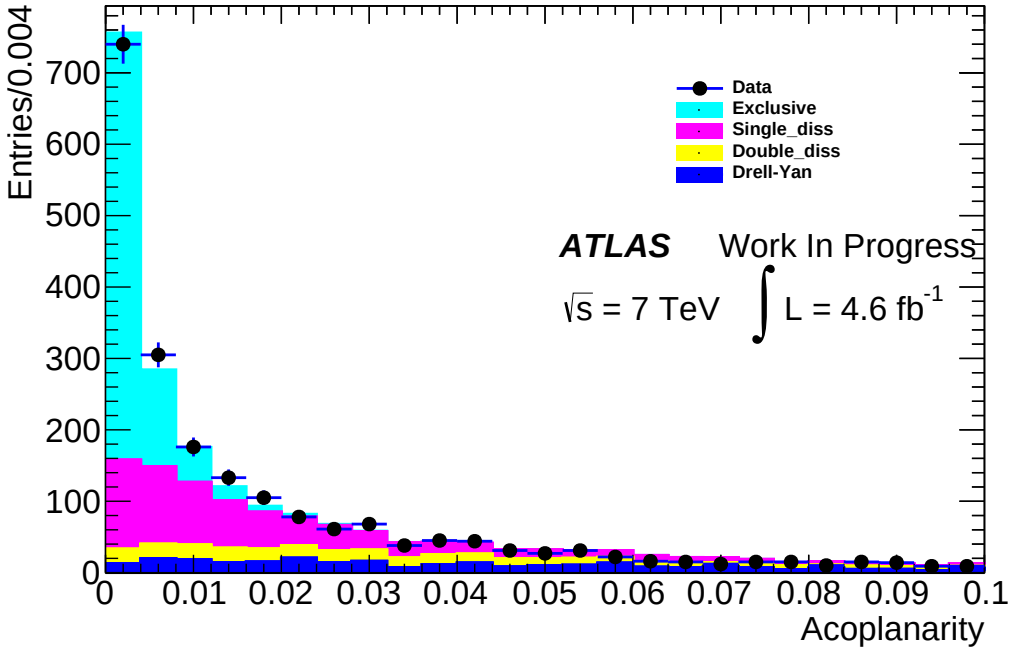

FIGURE 4.5: Acoplanarity of di-muon pair with scaling factor applied for the PYTHIA8 double dissociative case. Uncertainty in data represented by error bars.

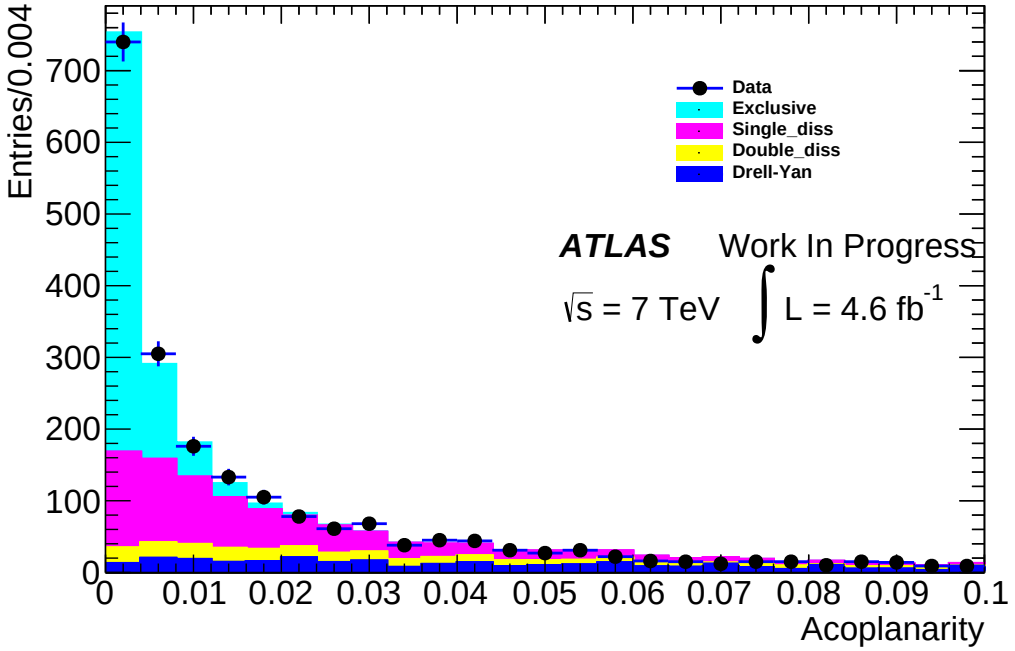

FIGURE 4.6: Acoplanarity of di-muon pair with scaling factor applied for the LPAIR 4.0 double dissociative case

As can be seen from Figure 4.6 and Figure 4.5 the findings are similar. From this we can conclude that there is no significant bias from the generator used and the PYTHIA8 double dissociative sample is used from here on.

The fit was done on the acoplanarity alone, with the other variables not being taken into consideration. The other variables were kept as "control distributions" in order to ensure that the ratios obtained from the fit are valid in all variables.

The cut flow values were now adjusted to the reflect the scaling and can be found in Table 4.3.

TABLE 4.3: Cut Flow Table with Scaling Applied

Selection Criteria	Data	Exclusive	Single Diss.	Double Diss.	Drell-Yan	Total MC
Preselection	7559306	4014	6429	10057	1444490	1464989
Same vertex	62492	1011	1613	1590	21003	25218
Two Tracks	4497	862	1368	689	1086	4007
Vertex exclusivity	3347	826	1310	631	639	3406
Δp_T	2214	808	783	312	302	2206
Acoplanarity	1168	755	288	52	38	1134

Control Distributions

In order to gain confidence in the validity of our fit we examine the distributions of other parameters. These distributions were not fit, and used the same scaling factors applied to the acoplanarity distribution. As can be seen in all the following figures the Monte Carlo and data agree well, giving us reason to be confident in the validity of our fit.

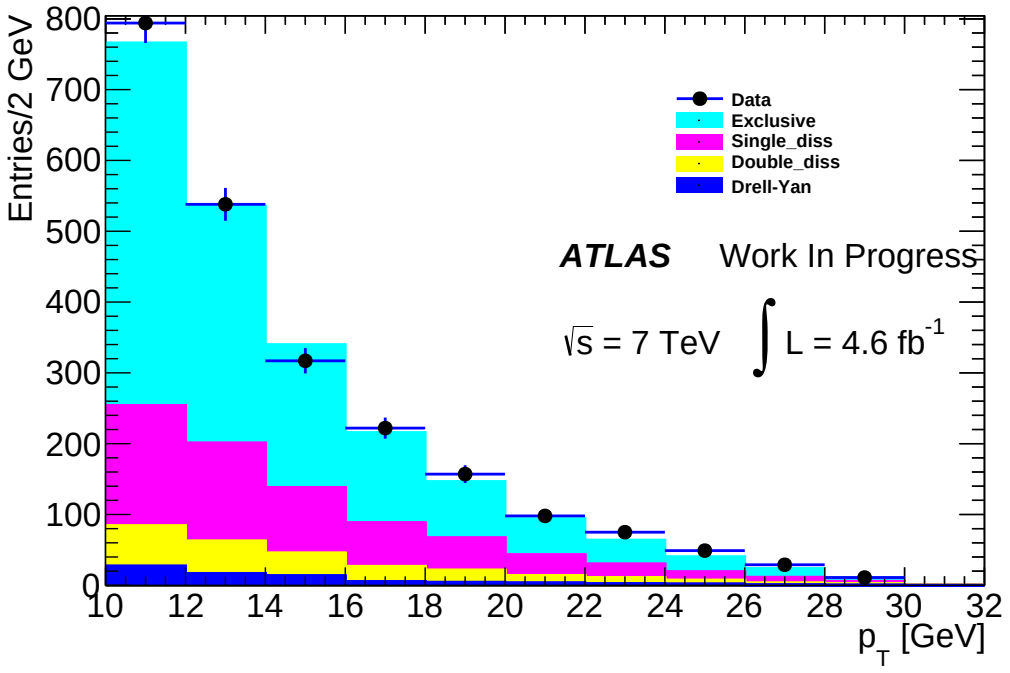

FIGURE 4.7: Transverse Momentum of the di-muon pair with scaling applied

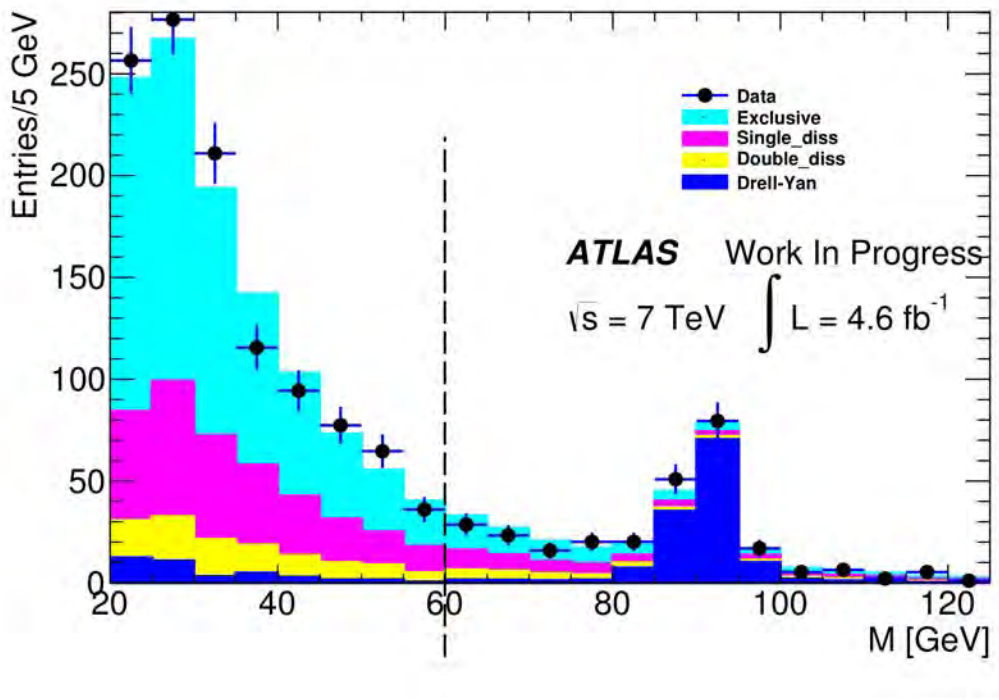

FIGURE 4.8: Invariant Mass of the di-muon pair with scaling applied. The invariant mass range to the left of the dotted line was studied, while the higher invariant mass range is added here for verification purposes

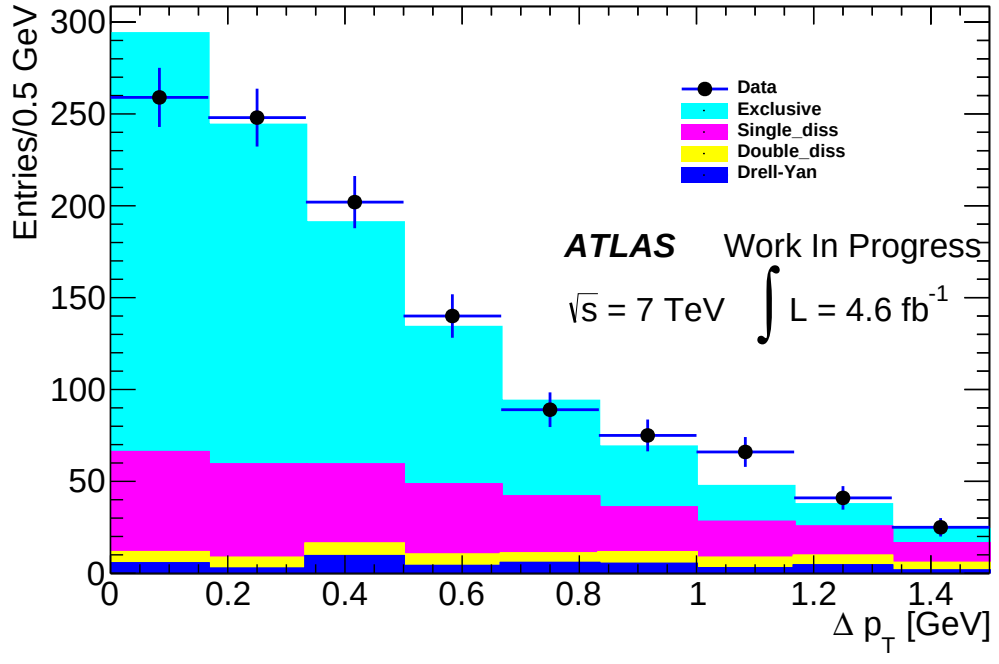

FIGURE 4.9: Δp_T of the di-muon pair with scaling applied

Cross Section

The cross section was calculated using:

$$\sigma = \frac{N_s}{A\varepsilon \int \mathcal{L}dt} \tag{4.2}$$

Where $N_s = N_o - N_b = 755$. N_s is the number of muon pairs from our signal process, N_o is the total number of muon pairs and N_b is the number of muon pairs from background processes. ε, the efficiency, and A, the acceptance ware determined from Monte-Carlo and $\varepsilon A = 0.17$. The integrated luminosity used was $\int \mathcal{L}dt = 4.6$ fb^{-1}.
The cross section was found to be 0.98 pb^{-1}, compared to a theoretical prediction of 1.07 pb^{-1}.

4.4 Systematic Uncertainties

As there are several steps in the process of measuring a cross section there are also uncertainties in these steps. The following is an assessment of the various uncertainties that affect this measurement.

Luminosity

The uncertainty in luminosity has been calculated in a study by the ATLAS collaboration using luminosity sensitive detectors. The uncertainty due to luminosity was found to be 1.8%[39].

Muon Reconstruction

There are several uncertainties associated with muon reconstruction such as the uncertainty in the muon trigger efficiency and the muon reconstruction efficiency. In general these efficiencies are very high, being around 99% for muon reconstruction efficiency for muons with $5 \lesssim p_T \lesssim 100$ GeV with uncertainties of $\pm$ 0.05% to $\pm$ 0.2% depending on rapidity [40]. Similar studies with similar muon requirements to this study[41] the total uncertainty for the muon system is significantly less than 1%. So a conservative

estimate is taken and 1% is added to the total uncertainty of the cross section.

Background

As the measurement of the cross section relies on the accuracy of the models of the background processes, there will be an uncertainty related to the effects of the background on the fit. To determine what effect the background has on the measurement the scaling of the Drell-Yan and double dissociative backgrounds were varied up and down by 50% in order to ascertain the effect a large variation in background would have on the total measurement. There is no fundamental reason for choosing 50%, it is just a factor much larger than any possible uncertainty that the backgrounds might have. The effect was found to be relatively small, with a 1.4% uncertainty due to the double dissociative background and a 0.8% uncertainty due to the Drell-Yan. This small variation shows that the final results found are not very sensitive to any possible uncertainties that might exist in the background Monte Carlo samples.

Fit Stability

As a fitting procedure was used there will be some uncertainly due to the fit. In order to ensure that the fitting was stable, the number of bins was varied during the fitting procedure. The maximum uncertainty due to fitting was found to be 2.7%.

Model Dependence

As two different generators were used for the double dissociative contribution an estimation for generator model dependence can be found, and the maximum discrepancy found was 2.1%.

Vertex Exclusivity

For the selection criterion on the distance between the candidate exclusive vertex and the nearest vertex, the distance parameter was varied over a sample of values between 2 mm and 5 mm to find the effect on the final amount of passing muon pairs in both

Monte Carlo and data. A maximum discrepancy of 2.0% was found.

4.5 Total Uncertainties

TABLE 4.4: Total Uncertainty

Luminosity	1.8%
Muon System	1.0%
DY Background	0.8%
DDiss Background	1.4%
Fit stability	2.7%
Model dependence	2.1%
Vertex exclusivity	2.0%
Total Systematic	4.7%
Statistical Uncertainty	6.1%

4.6 Results

The resulting cross section for exclusive $\gamma\gamma \to \mu\mu$ at 7 TeV from a fit to the acoplanarity is found to be 0.98 $\pm$ 0.06 (stat.) $\pm$ 0.05 (syst.) pb^{-1}. The predicted cross section is 1.08 $\pm$ 0.01 (theory) pb^{-1}. From the fit the data-theory ratio was found to be 0.91 for the exclusive case, which is similar to the value of $0.83^{+0.14}_{-0.13}$(stat.) $\pm$0.04(syst.)$\pm$0.03(lumi.) found by the CMS collaboration[22] and on the same order as the survival factor predicted in [21].

Chapter 5

Conclusion

Exclusive two-photon production is an interesting process that can be studied at particle colliders and the LHC in particular. The theory of exclusive production is a theory that has come a long way and has been tested at several experiments, including CMS, CDF and HERA. The theory relies on charged particle interactions, and is not limited to hadrons, but the use of hadrons does mean that more complex effects due to the structure of the proton need to be taken into account. The process of purely exclusive production has a fairly low cross section, meaning the LHC with its high luminosities is currently the most useful collider when it comes to studying these interactions. The CDF experiment at Fermilab only observed around 80 exclusive candidate events in 1.48 fb^{-1} of proton-antiproton data, whereas this study sees an order of magnitude more candidates, significantly improving the statistical significance of the measurements.

Similar to the method used by the CMS experiment[22] selection criteria based on the kinematic characteristics of exclusive interactions are applied to the 2011 dataset from the ATLAS experiment, with the difference that other than the CMS study, which required a no-pileup environment, this study was done with pileup and shows that as long as measures are put in place to prevent signal contamination due to pileup, studies such as this can be done in a pileup environment. The measures put in place rely on the vertex exclusivity and the vetoing of any vertex with more than two tracks originating from it, both of which take advantage of the ALTAS detector's accurate tracking capabilities. As a result it shows that it might be possible to do a similar measurement at the higher instantaneous luminosities of Run II and beyond.

The measurement of the photon mediated exclusive cross section for the production of muon pairs in 4.6 fb^{-1} of ATLAS data at $\sqrt{s} = 7$ TeV for the invariant mass range of 20 to 60 GeV is reported. $\sigma(pp \to p\mu^+\mu^- p)$ is found to be 0.98 $\pm$ 0.06 (stat.) $\pm$ 0.05 (syst.) pb^{-1}.

A discrepancy of (on average) about 10% was found between the predicted and found cross sections of the exclusive production, as well as significant discrepancies between the predicted and found dissociative cases of on the order of 20-30%. It is difficult to disentangle these discrepancies as these processes are so closely related. One would expect if the proton broke apart more often than predicted this would mean that less exclusive event should be found, while more single and double dissociative samples would be found, as a exclusive event in which one proton fails would then become an single dissociative event.

We can conclude that there is some evidence that the Monte Carlo generators used have some shortcoming when it comes to predicting the behaviour of photon mediated interactions, but whether this is due to the assumptions in the Equivalent Photon Approximation not being valid at the current energies, or whether the full understanding of photon PDFs is lacking remains to be seen[21].

It seems possible that a similar analysis can be repeated at higher energies and luminosities, which could provide more signal events and better statistics. An interesting and somewhat similar analysis that can be done is the measurement of exclusive two photon production of W^+W^- bosons, as done by CMS in [42], where two events were found. Again, this was done in the absence of pile-up. The possibility of doing such an analysis in a pile-up environment is given credence by this thesis and [35] and would allow for this analysis to be extended to higher energies an luminosities which will produce much higher signal events.

Appendix A

Data and Monte Carlo Used

Below is a list of the Data and Monte Carlo used and their properties.

Data:

`data11_7TeV.period*.physics_Muons.PhysCont.NTUP_SMWZ.grp10_v01_p1035/`

Where * is B, D, E, F, G, H, I, J, K, L, M.

Monte Carlo:

`mc11_7TeV.185337.Herwigpp_QED_ggTOmumu_20M60_LeptonFilter.merge.NTUP_SMWZ.e2456_a186_s1571_a145_r2993_p1035/`

`mc11_7TeV.185346.LPair_BSY_SDiss_ggTOmumu_20M60_LeptonFilter.merge.NTUP_SMWZ.e2456_a186_s1571_a145_r2993_p1035/`

`mc11_7TeV.185349.LPair_BSY_DDiss_ggTOee_20M60_LeptonFilter.merge.NTUP_SMWZ.e2456_a186_s1571_a145_r2993_p1035/`

`mc11_7TeV.129661.Pythia8_MRST2004QED_ggTOmumu_20M60_LeptonFilter.merge.NTUP_SMWZ.e2153_s1570_s1571_r3108_r3109_p1035/`

`mc11_7TeV.185607.PowHegDYmuPythia_20M38_DiLeptonFilter.merge.NTUP_SMWZ.e2875_a131_s1353_a145_r2993/`

`mc11_7TeV.108304.PowHegZmuPythia.merge.NTUP_SMWZ.e825_s1372_s1370_r3043_r2993_p1035/`

`mc11_7TeV.129807.PowHegDYmuPythia.merge.NTUP_SMWZ.e1423_s1372_s1370_r3108_r3109_p1035/`

Bibliography

[1] F. Halzen and A. D. Martin, *QUARKS AND LEPTONS: AN INTRODUCTORY COURSE IN MODERN PARTICLE PHYSICS* (Wiley, New York, USA, 1984).

[2] L. Evans and P. Bryant, JINST **3**, S08001 (2008).

[3] ATLAS Collaboration, JINST **3**, S08003 (2008).

[4] ATLAS Collaboration, Phys.Lett. **B716**, 1 (2012), arXiv:1207.7214.

[5] CMS Collaboration, Phys.Lett. **B716**, 30 (2012), arXiv:1207.7235.

[6] Standard Model Particles, 2011.

[7] E. Fermi, Zeitschrift für Physik **88**, 161 (1934).

[8] S. Glashow, Nucl.Phys. **22**, 579 (1961).

[9] S. Weinberg, Phys.Rev.Lett. **19**, 1264 (1967).

[10] A. Salam, Conf.Proc. **C680519**, 367 (1968).

[11] V. Budnev, I. Ginzburg, G. Meledin, and V. Serbo, Nucl.Phys. **B63**, 519 (1973).

[12] V. Budnev, I. Ginzburg, G. Meledin, and V. Serbo, Phys.Rept. **15**, 181 (1975).

[13] K. Piotrzkowski, Phys.Rev. **D63**, 071502 (2001), arXiv:hep-ex/0009065.

[14] P. J. Mohr, B. N. Taylor, and D. B. Newell, Rev. Mod. Phys. **84**, 1527 (2012).

[15] D. d'Enterria and J.-P. Lansberg, Phys.Rev. **D81**, 014004 (2010), arXiv:0909.3047.

[16] S. Drell and T.-M. Yan, Phys.Rev.Lett. **25**, 316 (1970).

[17] M. Gigg and P. Richardson, (2007), arXiv:0706.2921.

[18] S. Baranov, O. Duenger, H. Shooshtari, and J. Vermaseren, (1991).

[19] T. Sjostrand, S. Mrenna, and P. Z. Skands, JHEP **0605**, 026 (2006), arXiv:hep-ph/0603175.

[20] Øystein Alvestad, Exclusive two-photon production of lepton pairs in PYTHIA8, Master's thesis, Norwegian University of Science and Technology, Trondheim, 2010.

[21] M. Dyndal and L. Schoeffel, Phys.Lett. **B741**, 66 (2015), arXiv:1410.2983.

[22] CMS Collaboration, JHEP **1201**, 052 (2012), arXiv:1111.5536.

[23] CDF, Phys.Rev.Lett. **98**, 112001 (2007), arXiv:hep-ex/0611040.

[24] CDF, T. Aaltonen *et al.*, Phys.Rev.Lett. **102**, 242001 (2009), arXiv:0902.1271.

[25] F. Marcastel, (2013), General Photo.

[26] C. H. for the Linac machine supervisors, The cern hadron ion sources, 1999.

[27] J. Pequenao, Computer generated image of the whole ATLAS detector, 2008.

[28] ATLAS TRT, V. A. Mitsou, p. 497 (2003), arXiv:hep-ex/0311058.

[29] J. Pequenao, Computer generated image of the ATLAS inner detector, 2008.

[30] Physik in unserer Zeit **6**, 130 (1975).

[31] J. Pequenao, Computer Generated image of the ATLAS calorimeter, 2008.

[32] Particle Data Group, J. Beringer *et al.*, Phys.Rev. **D86**, 324 (2012).

[33] J. Pequenao and P. Schaffner, An computer generated image representing how ATLAS detects particles, 2013.

[34] GEANT4, S. Agostinelli *et al.*, Nucl.Instrum.Meth. **A506**, 250 (2003).

[35] ATLAS, (2015), arXiv:1506.07098.

[36] NNPDF, R. D. Ball *et al.*, Nucl. Phys. **B877**, 290 (2013), arXiv:1308.0598.

[37] M. working group, CERN Report No. ATL-COM-PHYS-2012-716, 2012 (unpublished).

[38] W. Verkerke and D. P. Kirkby, eConf **C0303241**, MOLT007 (2003), arXiv:physics/0306116, [,186(2003)].

[39] ATLAS, Eur.Phys.J. **C73**, 2518 (2013), arXiv:1302.4393.

[40] ATLAS, Eur.Phys.J. **C74**, 3130 (2014), arXiv:1407.3935.

[41] ATLAS, JHEP **1406**, 112 (2014), arXiv:1404.1212.

[42] CMS, JHEP **07**, 116 (2013), arXiv:1305.5596.